Deutsches Zentrum
für Luft-
und Raumfahrt e. V.

Institute for Aerodynamics
and Flow Technology
Göttingen

Report DLR-IB-AS-GO-2017-153

Author M. Rütten, S. Koch

Title

MTT Test Report

3D-Adaptation Procedure for the 2D-Adaptive Walls in the DNW-KRG Test Section

Program : LAR 387
Customer : MTT
Kostenträger : 3 006 579

Accessibility : ☐ I free ■ II int. free ext. restricted ☐ III int. restricted ext. restricted ☐ IV confidential

Distribution : 3x MTT
5x AS-HGK
5x Reserve

Report contains : 38 Pages incl.
5 Tables
9 References
23 Figures

Document source : Place : Göttingen
Department : AS-HGK
Date : 17.07.2018

Institute head	Department head	Author	Author
Prof. A. Dillmann	Dr. K. Richter	Dr. M. Rütten	Dr. S. Koch

Abstract

The Business Unit GUK of DNW proposed a research and development support in cooperation with the Institute of Aerodynamics and Flow Technology (DLR–AS) entitled “3D-Adaptation Procedure for the 2D-Adaptive Walls in the DNW-KRG Test Section”. The research objective was to verify an existing 3D-adaptation procedure at the Cryogenic Ludwieg Tube Gttingen (DNW-KRG) which allows an optimal adjustment of the test sections 2D-adaptive walls to achieve a minimum of wall interference during measurements with a built-in 3D-object.

Contents

Symbols

b	Model span
c	Chord length
c_r	Chord length at wing root
c_t	Chord length at wing tip
C_d	Drag coefficient
C_l	Lift coefficient
C_p	Pressure coefficient
d_c	Cylinder diameter
d_r	Maximal profile thickness at wing root
d_s	sting diameter
d_t	Maximal profile thickness at wing tip
h	Test section height
l_{ec}	Elliptic cone section length
l_c	Cylinder length
l_s	sting length
M	Mach number
Re	Reynolds number with chord length as reference
x	Chordwise location
y	Spanwise location
y^+	Dimensionless wall distance of first field grid point
z	Location normal to x and y

Greek Symbols

α	Model angle of attack
ϕ	Camberline sweep angle
ϕ_{le}	Leading edge sweep angle
ϕ_{te}	Trailing edge sweep angle

Indices

c	Charge condition
0	Stagnation condition
p	pressure
∞	Free stream condition

Abbreviations

AOA	Angle of attack
AUSM	Advection Upstream Splitting Method
CAD	Computer Aided Design
CFD	Computational Fluid Dynamics
CFL	Courant-Friedrichs-Lewy
DLR	Deutsches Zentrum für Luft- und Raumfahrt (German Aerospace Center)

DNW	Deutsch-Niederländische Windkanäle (German-Dutch Wind Tunnels)
KRG	Kryo-Rohrwindkanal Göttingen (Cryogenic Ludwieg-Tube Göttingen)
LB	Lifting Body
NTF	National Transonic Facility, NASA Langley Research Center
MG	Multi Grid
RAE	Royal Aircraft Establishment
SAE	Spalart-Allmaras turbulence model with Edwards modification
SAE-neg	SAE turbulence model with negative vortex correction
SST	shear stress tensor
TAU	DLR flow solver
TCT	Transonic Cryogenic Tunnel, NASA Langley Research Center
V3	multi-grid stepping scheme
Wilcox k-ω	turbulence model

List of Figures

List of Tables

1 Introduction

When investigating the flow around scaled aircraft model configurations in transonic wind tunnel tests, it is necessary to change the wind-tunnel test-section wall geometries in order to manipulate the flow in such a way that the model, to be tested, experiences the same flow conditions as the same model under free stream conditions. This is called “wall adaptation”. This wind tunnel technique works very well and, thus, wall adaptation devices can be found in many wind tunnel facilities. However, since the change of the wall geometries respectively contours are realized by some mechanical devices, the degree of freedom in controlling the wall contour is limited. Furthermore, it is extremely difficult to adapt all walls of the wind tunnel test section, surrounding the wind tunnel model, to suppress the repercussion of the test section walls on the flow around the model. More freedom in designing a flow field is always desirable, but in reality mechanical restrictions have to be faced. Therefore, in most wind tunnel test facilities wall adaptation is only conducted for the “lower” and “upper” test section wall assuming an associated aerodynamic model coordinate system, where the upper wall lays on the suction side and the lower wall on the pressure side. This is the very common and successful set-up.
Not least due to the mechanical complexity but also due to the financial efforts, in most wind tunnels, in which test-section wall-contour adaptation is available, the wall deformation itself is restricted only to a two-dimensional wall contour change in mean flow direction. This means that the wall deformation in span-wise direction is kept the same, which is called quasi two-dimensional or 2.5–D deformation. It is obvious that this deformation simplification does not fit to complex 3D wind tunnel models. For those cases a 3D-adaptation program is implemented in the environment of the KRG data analysis tool ”dark” using wall pressure distributions and wall shapes, adjusting the 2D-walls for a 3D-object in the KRG’s test section. So in the following it has to be ascertained and validated that it is possible that the wind tunnel flow around complex 3D models can be kept free from those disturbances using a special 2D-wall-contour despite of the three-dimensional character of the model. If this is ideally the case, then the result of the wall adaptation is the “interference-free wall contour”.
In order to clarify this essential issue this study investigates a very generic aircraft configuration in the Kryo-Rohrwindkanal Göttingen (Cryogenic Ludwieg-Tube Göttingen) (KRG) of the DNW. The reason why to consider a generic configuration was that the results of the exploration should be useful for various aircraft wind tunnel model investigations. Therefore, stereotypical elements of modern aircraft were reproduced in the investigated wind tunnel model, the relatively huge long cylindrical body with a sharp head representing the fuselage, and the typically weakly swept thin wing mounted at the middle section of the fuselage. Additionally, the wind tunnel model sting, which is used to place or to move the model at or to a certain position, is also considered. This is necessary, since possible flow blockage effects due to the model mount have to be faced by the wall adaptation procedure.
This report describes the CFD study, in which the impact of a controlled DNW–KRG wall-contour adaptation on the flow around the model is numerically replicated. Thereto, first the wind tunnel and aircraft model configuration are introduced, then, the numerical simulation tools and simulation set-up are explained. Thereafter, the applied specific wall-contour adaptation strategy, which follows the same procedure as used during the wind tunnel experiments, is discussed in detail. This report ends with a final evaluation of the CFD results.

2 Wind Tunnel and Aircraft Configuration

The following subsection describes the Cryogenic Ludwieg-Tube Göttingen (section 2.1), whose wall adaptation device was focal of interest. Then, the subsequent subsection introduces the considered generic aircraft configuration.

2.1 The Cryogenic Ludwieg-Tube Göttingen (DNW–KRG)

The DNW–KRG (Fig. 1) is a blow-down wind tunnel based on the Ludwieg-Tube concept [5] for high Reynolds number research in transonic flow. Operating at stagnation pressures up to 1 MPa and charge temperatures down to 100 K, it is possible to achieve Reynolds numbers up to 60×10^6 based on a model chord of 150 mm (2–D). In Fig. 2 the whole M,Re-envelope for this facility is shown. The Mach number in the test section is set using a control valve adjusting a sonic throat downstream of the test section. A detailed description of the DNW–KRG can be found in [6]. The test time of the DNW–KRG is between 0.6 s and 1.0 s, depending on the fluid temperature. Without any components upstream of the test section that may cause disturbances like an installed fan or turning vanes, a good flow quality is achieved. Additional information regarding the flow quality of the DNW–KRG as well as a comparison with other cryogenic facilities like the TCT or the NTF can be found in [4]. Depending on the charge pressure and temperature, 20 – 30 test runs can be executed per day. The test section has a

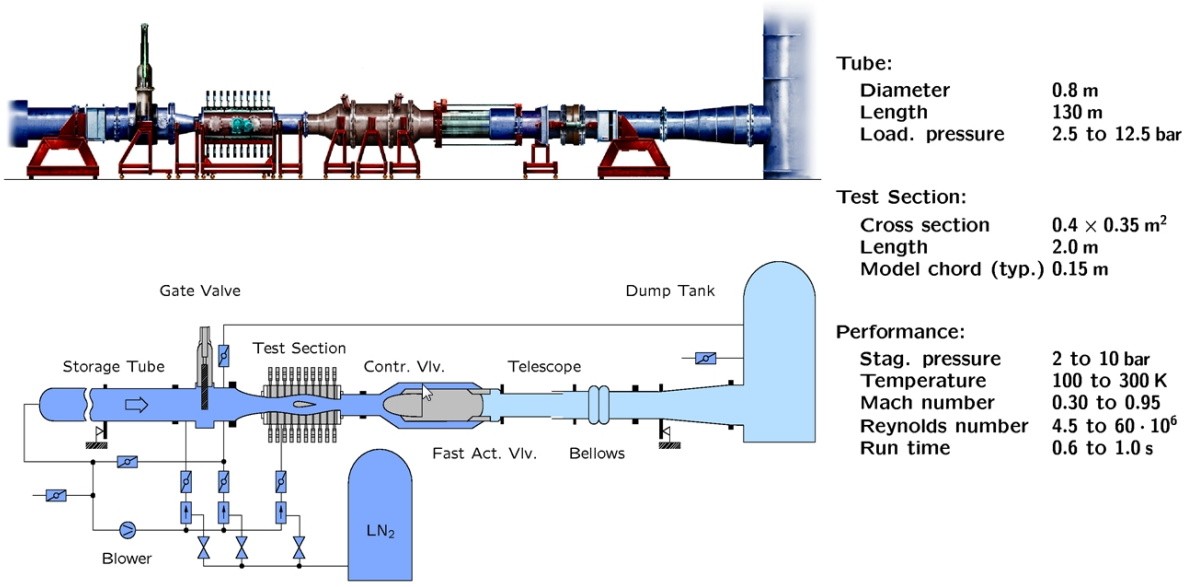

Figure 1: Schematic illustration of the Cryogenic Ludwieg-Tube Göttingen (DNW-KRG)

width of 400 mm and height of 350 mm and a test section length of 2000 mm. The position of the flexible upper and lower wall are determined by a non-iterative Cauchy method from the deflection of the walls and the wall pressure distribution. This procedure was first described in [6] for 2D flow case, ist is similar handled for 3D flows. For a test run with an interference free wall contour a second test run is necessary. However, under favourable conditions it is possible to determine the needed wall shapes by interpolation from test runs already completed.
Detailed CAD drawings and models of the DNW–KRG are available which allow to perform CAD cleaning processes necessary for the subsequent generation of associated CFD grids.

2.2 Lifting Body Aircraft Model

In a former experimental study to KRG wall adaptation, reported in [3], a lifting body (LB) model was developed which is nothing else than a very generic aircraft with a fuselage and wing section only. A sketch and technical data of the configuration can be found in Figure 3. It has to be remarked that the model used in KRG wind tunnel is scaled with the scaling factor of 1/2. The fuselage itself is split into a cylindrical part and an elliptic sharp cone building its tip. The

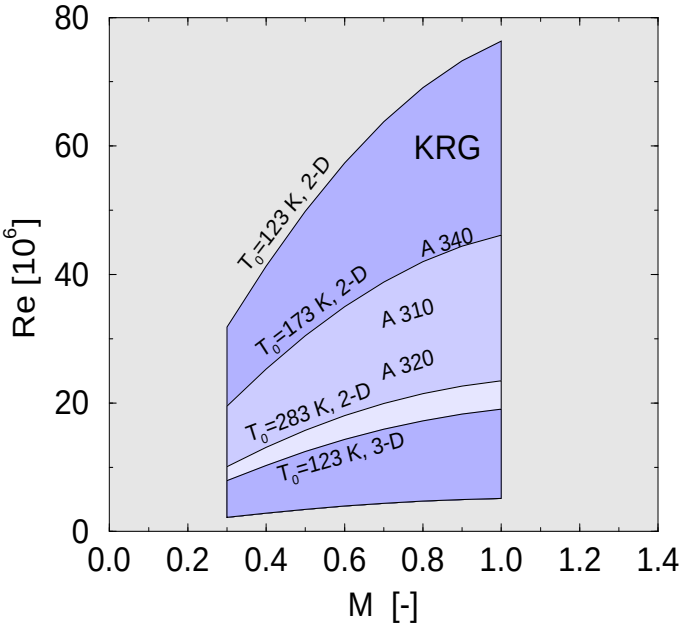

Figure 2: M, Re-diagram of the DNW-KRG

elliptic cone section is $l_{ec} = 120\,\text{mm}$ long, followed by the cylinder of a length of $l_c = 280\,\text{mm}$. The diameter of the cylinder is $d_c = 30\,\text{mm}$.

The wing geometry is based on a symmetric RAE 101 profile. In contrast to the original

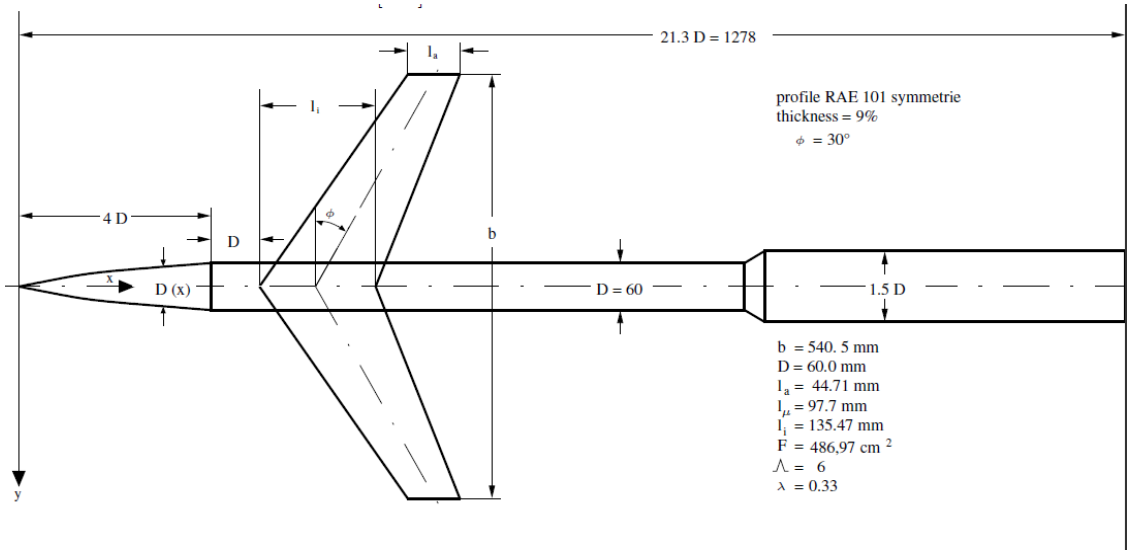

Figure 3: Scetch of the original LB model with technical data. Remark: KRK model scaled 1:2

geometryd described in [3] the airfoil has a rounded leading edge whereas the trailing edge is kept sharp. The swept wing is mounted at the 1/2 position of the cylindrical part of the fuselage at centerline height. The wing has a camberline sweep angle of $\phi = 30°$, this results in a sweep angle of the leading edge of $\phi_{le} = 34°$, the trailing edge is $\phi_{te} = 21°$ swept. The chord length of the wing at the wing root is $c_r = 62.7\,\text{mm}$, the chord length at the wing tip is $c_t = 22.355\,\text{mm}$. At the wing root the maximal profile thickness is $d_r = 6.25\,\text{mm}$, at the tip the maximal thickness is $d_t = 6.25\,\text{mm}$. The model span is $b = 270.25\,\text{mm}$.

The cylindrical sting, on which the LB model is mounted, is also modelled in the CAD representation. This is necessary to get more realistic flow conditions which are closer to the original experimental setup. However, the wind tunnel sword, on which the sting is originally mounted, is not taken into account in order to reduce the modelling and simulation effort. The represented sting part has a length of $l_s = 476\,\text{mm}$ and a diameter of $d_s = 45\,\text{mm}$. A 45° cone element is used as connector to the fuselage. For getting a visual impression a CAD sketch of the LB model is depicted in Figure 4. Further geometry information can be found in the internal DLR report

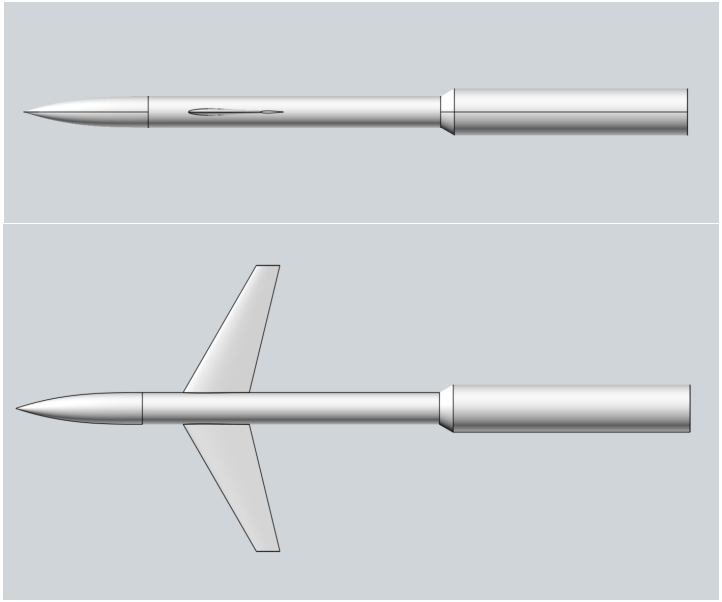

Figure 4: CAD drawing of the LB model, side and top view.

[3]. It has to be remarked that the term "lifting body", which was used in former projects is misleading, since the symmetric body and wing configuration can not produce lift in neutral position at an AoA of $\alpha = 0°$. Thus, this configuration can only generate lift if the AoA is increased, thus, the lift function is dominated by the AOA.

3 CFD Simulation Study

As mentioned above, the task of the CFD study is to investigate the influence of wall adaptation on the resulting flow around the generic fuselage-wing configuration mounted in the test section of the KRG wind tunnel. It shall be shown whether CFD can reproduce the wall adaptation procedure conducted during a typical wind tunnel experiment in order to minimize the wind tunnel wall impact on the flow around the configuration. Numerical flow simulations were performed for various flow conditions. For this purpose the Navier-Stokes solver TAU of the DLR [2], [9] (Version Release.2014.1.1) was employed for three-dimensional computations.
The CFD simulation study itself was performed in two steps: in the first step the steady flow around the generic LB aircraft was investigated under the aspect of the flow sensitivity to the wall adaptation itself. This step was necessary in order to proof whether the LB-KRG configuration was a suitable test case for the investigation of flow effects induced by the wall-contour adaptation of only a single (here the lower) wall within the test section. Only when a sensitivity could be observed the next step could be made.
Focal point of the second step of the simulation study was to investigate the sensitivity of the flow field in the nearfield of the generic LB aircraft configuration to especially controlled wall-contour changes. This second part of the study mimicked the special wall adaptation procedure

commonly conducted during DNW–KRG experiments in which the flow around complex models is investigated, see [7]. The objective, now, was to numerically reproduce the procedure of the wall-contour adaptation technique used in experiments and, therewith, to show the validity of this overall work flow. In the second part of the study, both the lower and upper wall contours were deformed.
For the latter purpose two simulation lines are followed: in the first the generic LB aircraft was mounted within the test section of the KRG with an angle of attack (AoA) of $\alpha = 0°$, but the upper and lower test sections walls were differently pre-deformed. Here the goal was to show, that the wall adaptation procedure, numerically reproduced, will lead to nearly symmetrically shaped test section wall contours due to the expected symmetric flow. It is not expected that the resulting wall contours will be exactly mirrorable, since a certain robustness of the flow against small deviations can be assumed, nevertheless, the final contours should be quite similar.
In the second simulation line the wind tunnel model got an AoA of $\alpha = 3°$ prescribed, which indeed means that, as in the wind tunnel experiment, the model has to be rotated around the span-wise axis by 3°. The idea behind was, that now, the wall adaptation procedure should finally reproduce a test section wall contour which minimizes the wall effects leading to quasi freeflight conditions. Eventually this means that as result of the performed CFD study the same C_p distribution shall be achieved for first the generic LB aircraft configuration flow case simulated under free flight conditions and second the well wall-adapted KRG flow simulation case with the LB configuration in the wind tunnel test section.
Before discussing the CFD simulation study results, the used CFD tools and the simulation strategy have to be explained, this is the main task of the next subsection. Properties of the flow solver TAU are first introduced, then, the CAD representation of the wind tunnel and the associated grid generation are discussed. Thereafter, the detailed simulation set-up from boundary conditions to solver settings is explained.

3.1 Flow Solver TAU

As mentioned the simulation study of the flow around the LB mounted in the test section of the KRG wind tunnel was conducted using the compressible solver TAU [9] , which is the standard flow solver of DLR. The code has a second order spatial and temporal discretisation, it is well validated by a variety of experimental and numerical validation campaigns and is state of the art in regard to performance, efficiency and accuracy [8] . TAU is based on the finite volume (FV) method. Between two FV implementations can be chosen, the cell center or the dual grid respectively edge-based approach, whereas the latter one is the common one due to a currently easier and faster grid generation process for complex geometries. Different inviscid flux discretisation types are implemented: upwind, central or mixed schemes. Due to stability reasons in most flow simulation cases upwind fluxes, commonly AUSM (Advection Upstream Splitting Method) or Roe based schemes, are used. Runge-Kutta or Backward-Euler solver can be used as relaxation solvers. Linear relaxation can also be done by an adjoint version. Gradients are reconstructed by using the Green-Gauss or the least-square scheme. Stability can also be gained by certain central dissipation fluxes methods: the “scalar dissipation” and “matrix dissipation”. Additionally two different kind of central convective meanflow fluxes, the “average of flux” and the “flux of average” are implemented. For further stabilization one can select between different explicit and implicit smoothers: the “point explicit”, the “upwind implicit“, the “point implicit“, the “line implicit“ and the “first order implicit” smoother. With that variety of implemented methods one is able to simulate the flow even in or around very complex 3D configurations.

3.2 Simulation Setup of the Flow within the KRG Wind Tunnel Configuration

Since the generic LB aircraft model and wind tunnel wall-contour flow interaction are the focal point, the next sections are providing insight into the flow simulation reflecting the original KRG wind tunnel experiment. Details to the CAD configuration and grid generation are delivered. Thereafter, details of the simulation set-up in regard to solver settings and the performed simulation strategy are explained.

3.3 CAD and Grid Generation

The complete cryogenic wind tunnel is a very huge facility, thus, it was not practical to simulate the flow in the entire KRG wind tunnel. Due to its enormous length, the numerical flow simulation domain had to be restricted to those essential parts of the wind tunnel which are determining the flow field in the test section. Eventually for this CFD study the geometrically shortened CAD representation of the wind tunnel with the integrated generic LB aircraft configuration ranges from the gate valve to the fast act valve (see Figure 1). At the gate valve the tunnel is of cylindrical shape and has a diameter of 800 mm. A nozzle of a length of 1500 mm follows, it reduces not only the cross section significantly, it also changes the shape from a circular to a rectangular contour with a height of 350 mm and a width of 400 mm. The next and most important part is test section with the same rectangular cross section and a length of 2300 mm. The contour adaptive lower an upper wall parts a reaching from $x = 3.7\,\mathrm{m}$ to $x = 5.75\,\mathrm{m}$ The following section is a diffuser with a vertical mounted sword which carries the upstream pointing sting of a wake rake during 2D-profile experiments. The control valve of the cryogenic tunnel segment in which we are simulating the flow, is again cylindrical, having a diameter of 500 mm. This is the final part of the real wind tunnel taking into account. The CAD representation does not include the fast acting valve and subsequent parts behind. A CAD drawing of the computational domain is shown in Figure 5.

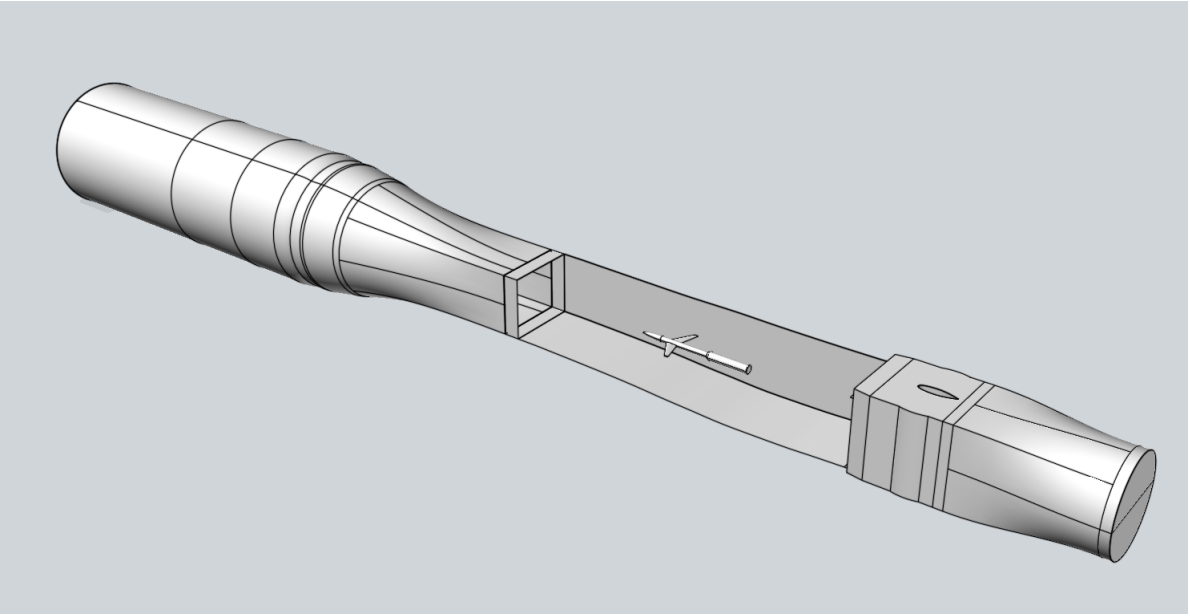

Figure 5: CAD drawing of the KRG wind tunnel, test section cutted free

The Figure 6 shows the integration of the generic LB aircraft model in the test section of the tunnel.

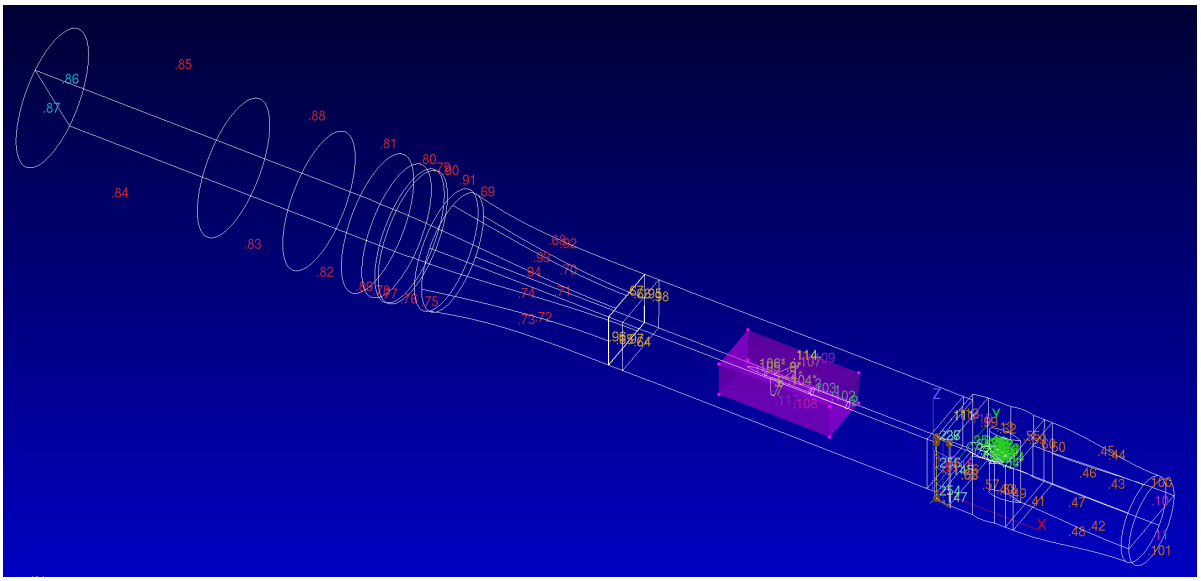

Figure 6: CAD view from CentaurSoft into the test section with highlighted LB model and grid source box.

For orientation a coordinate system was defined: its origin was placed at the beginning of CAD domain at the gate valve on the middle axis. The x-coordinate is pointing in stream down direction, the y-axis was pointing in width direction which corresponds to the so called span-wise direction of the LB aircraft configuration. Therewith the z-direction was defined as vertical axis. In this coordinate system the fuselage tip of the LB aircraft model was positioned at $x = 4790\,\text{mm}$ on the middle axis (y = 0.0 mm, z = 0.0 mm).
Although the considered part of the KRG wind tunnel was already reduced, the present configuration is still huge, therefore, from this figure it can be adumbrated the different geometric scales, which have to be faced in the performed CFD simulation study. This provides guidance to the grid generation which follows next.
The generation of the CFD mesh was conducted using the commercial grid generation tool "Centaur" from CentaurSoft. Several mesh and simulation pre-studies had to be performed: this was necessary, on the one hand, to find the adequate meshing parameters in order to achieve a high-quality grid necessary to resolve the boundary layer flow at the wind tunnel walls and around the LB configuration. On the other hand the fine spatial resolution at certain configuration parts is a pre-condition to resolve flow structures like near wall vortices with associated flow separation but more importantly flow shocks. In particular, the different length scales of the given configurations were challenging, since the simulated wind tunnel segment has a length of 7.0 m which is very long in relation to the boundary layer flow thickness around the LB fuselage in the range of mm.
For the CFD a hybrid grid generation approach has been chosen with different types of polynomial grid cells. The limiting outer and internal border of the flow domain are represented by surface triangles and quadrilaterals. Their size and shape varies over a wide range of scales, since lower spatial resolution is necessary at the gate and control valve flow regions, whilst high spatial resolution is necessary in the wing region of the test section. The flow domain is filled by tetrahedrons (tetras) and prismatic cells (prisms). The prisms are arranged in 32 pseudo structured layers, so called prism stacks. This high number of prism stacks is necessary to guarantee a fine spatial resolution close to the fuselage and wing surface and the wind tunnel walls. This is essential in order to resolve the boundary layer flow and, in particular, to enable an accurate calculation of the wall shear stress. The latter is crucial since only an accurate prediction of

Table 1: Parameter and Properties of CFD Grids

Parameter Grid Generation	
stretching ratio/growth factor surface elements	1.72
min./max. side length surface elements [mm]	0.08/50
factor for curvature clustering	13
factor for proximity clustering	8
factor for CAD clustering	4
initial value spacing	8.135
number prism layers	32
thickness of the first prism layer [mm]	0.019
stretching ratio/growth factor prism layers	1.14
ramp angle	8
stretching ratio/growth factor volume elements	1.6
interface length scales blending factor	0.8
interface thickness ratio	1.2

the wall shear stress allows to catch the right position of possibly occurring flow separation and shocks. The targeted objective of the study used for comparison, the C_p distribution on fuselage and wing, is directly depending on this. Therefore, the thinnest prisms are laying at the wall triangles, they grow slowly in wall normal direction, whereas the growth rate is consciously chosen small. Above the prims stacks tetras are filling up the CFD grid volume. Eventually, the locally pre-refined hybrid grids consisted of different types of polynomial grid elements, surface triangles and quadrilaterals, tetrahedral, prismatic and pyramidic volume cells (pyras). After generating the CFD grid this bunch of cells is transformed into a so called dual or edge-based grids in which the distinction in cell types is not necessary any more.
Another important aspect during the grid generation is the pre-definition of the spatial resolution around the generic LB aircraft. Since the flow around the LB configuration has to be resolved very accurately an additional source term box has been set around the configuration in order to increase the spatial resolution of the resulting CFD grid, well knowing that a lot of CFD grid points have to be additionally spent. However, without this grid refinement box flow results showed too less impact of the flow displacement from the generic aircraft on the wall. By setting this grid refinement source, defined as rectangular box, the grid cell sizes within the boxes were decreased significantly, which enabled the solver also to resolve the expected shock structure. It is necessary not only to increase the number of local grid cells at that flow region, where shock could be expected, it is also necessary to a high spatial resolution of the surrounding flow domain to allow the development of flow displacement up to the wall, in particular when considering compression effects at higher Mach numbers. The box respectively the grid refinement sources, is illustrated in the Figure 6. With this adjustments the grid generation was performed with regard to an onflow Mach number of $M = 0.8$. This transonic on-flow Mach number leads to very huge gradients of the flow velocity at and close the walls. These gradients have to be resolved which defines the needed spatial resolution there, and, therewith, the height of the first volume cell at the walls. Latter is very crucial, since this defines the so called y+ value, which is essential for the the validity and accuracy of applied turbulence models. By using analytic expressions and running cross-checks with preceding CFD simulation suitable values for the first layer heights were determined and set as parameter input in the final grid generation process. The most important grid generation parameters can be found in Table 1. To give an impression of the final CFD grid topology, in the Figures 7 and 8 detailed and cut sectional

views on grid sections are shown. After the grid study and the new grid generation process the

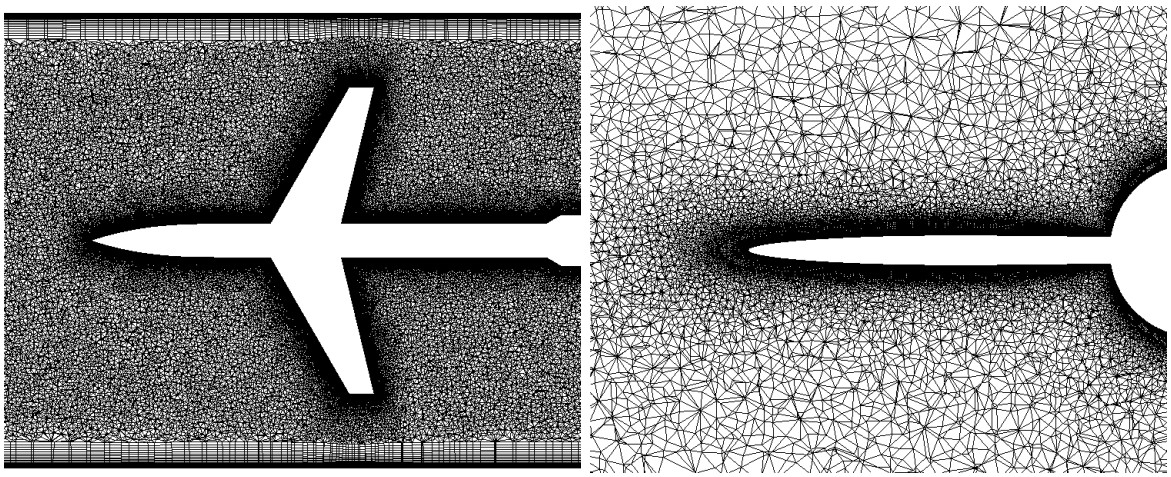

Figure 7: Illustration of the spatial resolution of the triangulated surface grid and pre-defined spatial resolution of the volume grid illustrated by a horizontal and vertical cutting plane.

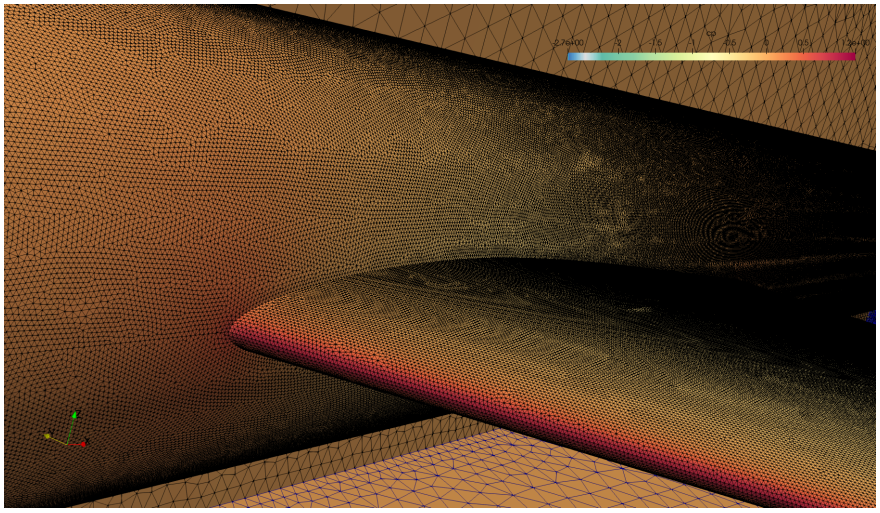

Figure 8: Grid quality: High spatial resolution of the CFD surface of the LB configuration, in particular the wing region is highly spatially resolved in order to reflect the airfoil curvature and, thus, to calculate the boundary layer flow accurately.

initial CFD grid for the 0° AoA flow case had 2961690 surface elements, 2940698 surface triangles and 20992 surface quads, 146714459 volume elements, 53295301 tetras, 93262467 prisms and 17641 pyras, and it consisted of 56684341 grid points. Since no points were added during the y^+ grid adaptation steps these numbers were also valid for the flow y+ adapted grids. It has to be remarked that during this CFD simulation a variety of CFD grids were generated, since wall contours and model alignment (AoA) had been changed, thus for each investigated flow case these numbers were different. However, since the parameters and source settings in CentaurSoft were not changed, all resulting grids had the same grid topology and their grid cell numbers were all in this range.

3.4 CFD Setup of flow around the generic LB aircraft within the KRG

The boundary conditions are the following: Nearly all grid surfaces were treated as so called "viscous walls" where the adhesion condition is valid. Total pressure conditions were set at the inflow plane and a certain static pressure at the exit plane according to the desired conditions with respect to Reynolds number and Mach number. By applying these boundary conditions it was possible to adjust the on-flow Mach numbers corresponding to the experiments conducted in the cryogenic wind tunnel. The onflow Mach number M_∞ was calculated as the mean value over five reference positions which were stemming from the pressure tab positions in the side wall, typically used in KRG wind tunnel experiments.However, in this virtual environment, the values were taken not at the side wall but along the middle axis of the test section. This procedure delivered an onflow velocity of around 251 m/s. With this value the Reynolds number was calculated to 6 million taking a Reynolds number reference length of $l = 0.15\,\mathrm{m}$. In the sensitivity study the pressure conditions were kept fixed, whereas wall contours and, as consequence, the onflow Mach number was changed. In the final study the opposite was done: the pressure conditions were changed to keep the onflow Mach number constant.
Modelling of turbulence, in particular for flow situations with separation, is still challenging. Here, the Spalart-Allmaras turbulence model with Edwards modification (SAE) [1] and negative formulated correction terms was used. For validation purposes the Wilcox k-ω turbulence model with the SST extension was also applied for cross-checking some flow cases. Comparing the numerical flow simulation results of both models showed nearly the same behaviour, thus, the SA-neg turbulence model was finally used, because its computational effort was lower.
An essential point for the numerical simulation of turbulent flows using turbulence models based on the Reynolds averaging approach is not only the turbulence model itself, the dimensionless y^+ value at the wall is also essential for the accuracy of the flow solution. Only if the y^+ value is in the range of one, RANS turbulence models are able to deliver valid Reynolds stress information for calculation of an accurate turbulent viscosity which is crucial for the determination of the turbulent viscous stress at the wall and eventually the C_p distribution on fuselage and wing parts. Therefore, a so-called y^+ value adaptation was performed which redistributed the

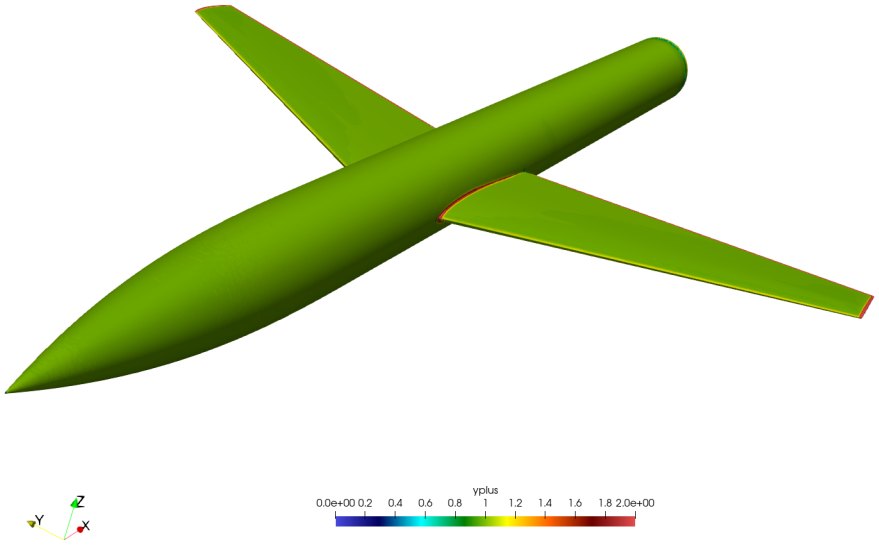

Figure 9: Grid quality study: y^+ values on the generic LB aircraft configuration.

prismatic layers in a way that a y^+ value distribution of nearly one at every surface point could be achieved. In Figure 9 the y^+ value distribution is shown as colour contour plot on the surface of the wind tunnel model. The y^+ values are in the optimal range, only at geometric corners of the model at the wing tip and at the fuselage-wing intersection y^+ values are occurring which are slightly too high. At those locations the calculations of the y^+ values are showing only an approximate value due to the well known double-face-normal computation-problem at sharp corners. Nevertheless, the CFD grid is accurately generated and fine enough spatially resolved so that the applied turbulence model is able to deliver valid data in the restricted framework of RANS modelling. It also has to be remarked that in the depicted image only the generic LB aircraft configuration is shown, the y^+ adaptation was, of course, applied to all wind tunnel walls, since all walls were assigned as viscous turbulent walls in the TAU framework and, therefore, treated by the y^+ algorithms.
Different numerical acceleration techniques were used. The flux splitting technique allowed to perform sub-iterations for simulation speed up. In addition, implicit residual averaging was performed to further accelerate the CFD calculations. Moreover, the multi-grid (MG) techniques was applied: after 500 pre-iterations the V3 scheme started on the finest level with eight relaxation steps between the MG-transfers and eight relaxation steps on the coarsest grid level. In this simulation study, simulations were performed assuming a steady flow, thus corresponding algorithm were used, though it is well known that flow separation, especially of vortical flows, can be highly unsteady. However, in the flow cases, considered here, it was assumed that unsteady flow phenomena are negligible and the global transonic flow features, as shocks, are dominant over smaller scale turbulent effects. Hence, in the CFD calculation setup the CFL number was set to 0.8. The calculations were performed on a Linux cluster using 200 cores. Each simulation was stopped when the residual declined by four orders, this was achieved after round about 12000 to 20000 iterations depending on the considered flow case. The computational effort was high due to the spatially fine resolving CFD grids with its 56 million grid points, thus, only 4000 to 60000 iterations could be computed during a 24 hour job, which means that a minimum number of three days were needed to get one intermediate CFD result. However, due to the needed y^+ adaptation step after each of two intermediate results and a fine-tuning of the static pressure value at the CFD domain exit-pressure-outlet boundary the computational effort was eventually much higher. This point was actually more crucial than thought before, and led to delays: The sensitivity to the slight changes of the wall resolution was very high, in particular for this wind tunnel. This led to the following procedure: after a first pre-calculation the y^+ adaptation was applied, thereafter, the simulation was restarted using the former solution as initial solution. Again after several thousand iterations a new steady solution could be achieved. It has to be noted that, then, it was also necessary again to adapt the pressure at the outflow boundary since a changed and - now - more accurate turbulent viscous drag at the wall, due to the conducted y^+ adaptation, led to other total pressure losses. This, however, made it necessary to repeat the CFD simulation and y^+ adaptation step again until a converged solution could be achieved. Again a fine-tuning of the exit-pressure setting was necessary to adjust the on-flow Mach number at given control respectively reference points, because better resolving wall shear stress due to the performed y^+ adaptation step changed even the flow behaviour in front of the model.

4 Results

In the following sections the results of the numerical simulation study are shown. At first the results of the sensitivity study will be discussed, thereafter the final results of the wall-contour adaptation procedure will be presented and explained.

Table 2: Five wall deformation types realized by the test section lower wall adaptation

Deformations and Cases	
V1	initial wall contour
V2	downstream one-sided wavy wall contour
V3	waek to stronger wavy wall contour
V4	strong wavy wall contour
V5	smoother wavy wall contour

Table 3: Mach Number Variation in the Sensitivity Study for Fixed Pressure Conditions

Mach Number for given Pressure Condition	
flow case	Mach number
V1	0.792
V2	0.815
V3	0.839
V4	0.828
V5	0.846

4.1 KRG Wall-Contour Adaptation Sensitivity Study Results

In order to proof the sensitivity of the chosen model to a performed wind-tunnel test section wall adaptation, at first the CFD results of the sensitivity study are shown and discussed.
This study started with the reference case, in which the lower and upper walls of the test section are kept straight. The calculated flow results were used as orientation fix point to reveal the dependence of the flow field on wall deformations. Hereto, this study concentrated on flow cases in which only the lower wall of the test section was deformed. Five different deformation types have been realized, see Table 2, the different deformation types are qualitatively described, exact CAD data of the deformed lower wall can be provided by the authors of the study. However, in order to get an impression of the lower test-section wall deformation, an illustration is delivered in Figure 10. In this study the outlet pressure was kept constant, this led to different onflow Mach numbers in front of the configuration, see Table 3 for the exact conditions. In the following picture series main focal point is laid on the C_p distributions on the upper and lower side of the generic LB aircraft configuration, since these are the main interesting objectives of aerodynamics and allow a visual comparison and assessment of the lower test-section wall-contour change on the flow field. Figure 11 shows the changes of the C_p distribution on the upper side of the LB fuselage and wing. The reference flow case (depicted with a part of the sting) reveals a typical C_p value distribution on the fuselage, from a relatively high value at the tip to lower values at the first curved fuselage parts and subsequent slightly higher values at the beginning of the straight fuselage part. then pressure is quite slowly decreasing. At the wing root the occurring flow acceleration over the wing leads to the expected pressure drop on the fuselage. Another obvious property of the reference configuration is the distinct suction region up to the first half of the airfoil that over the whole wing span.
When the lower test section wall contour is shifted towards the LB model in the front section the occurring blockage decelerates the flow leading to an globally increased pressure on the LB model surface. Opening the wall contour at the beginning of the test section, far in front of the wind tunnel model and narrowing the contour at the rear part of the model and behind leads

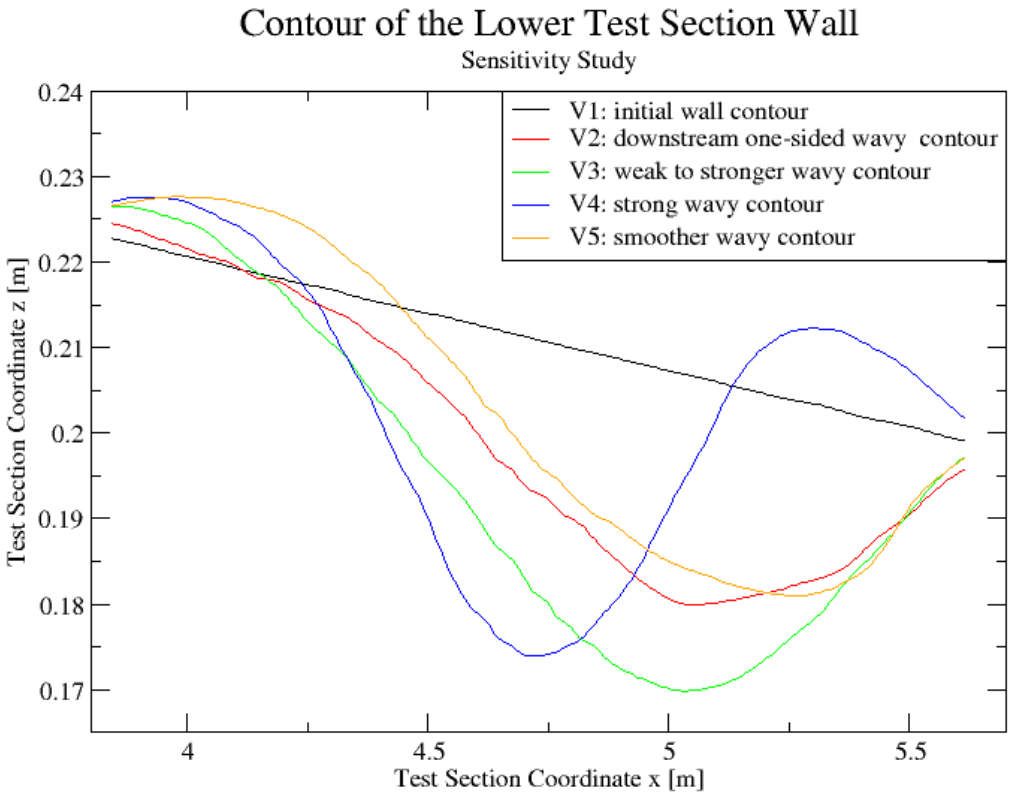

Figure 10: Visual impression of the deformation of the lower test section wall, the straight black line is the reference. (extracted at dicrete points - wrong impression of roughness)

to a crucial acceleration of the flow and a significantly reduced surface pressure with dominant suction peaks on wing. The opposite test section contouring leads to a decelerated flow and increased pressure values on the model. When comparing Figure 11 with Figure12, which shows the C_p distribution on the lower surface of the LB generic aircraft model, it is obvious that the described effects are more pronounced on the lower side as expected due the wall contour change there. The global behaviour of the flow above and below the model is the same: Eventually the observation of the depicted results reveals a strong sensitivity of the generic LB aircraft-model flow to the change of the wall contour. It can be observed that shifting the outwards directed contour bulge of the lower wall from upstream to downstream leads to a corresponding decrease on the C_p distribution.
It has to be remarked that further CFD studies with another strategy could be performed by extending the wall-contour adaptation parameter space in order to specify quantitatively the impact of geometrical wall contour changes on the C_p distribution on the generic aircraft model. However, this study only had in mind to proof, whether there is a sensitivity or not, and to show the suitability of the generic LB aircraft model for this CFD investigation, in which the real wind tunnel handling is followed virtually. As outcome of the study it can be stated that the chosen simulation setup is suitable for the objectives of the study.

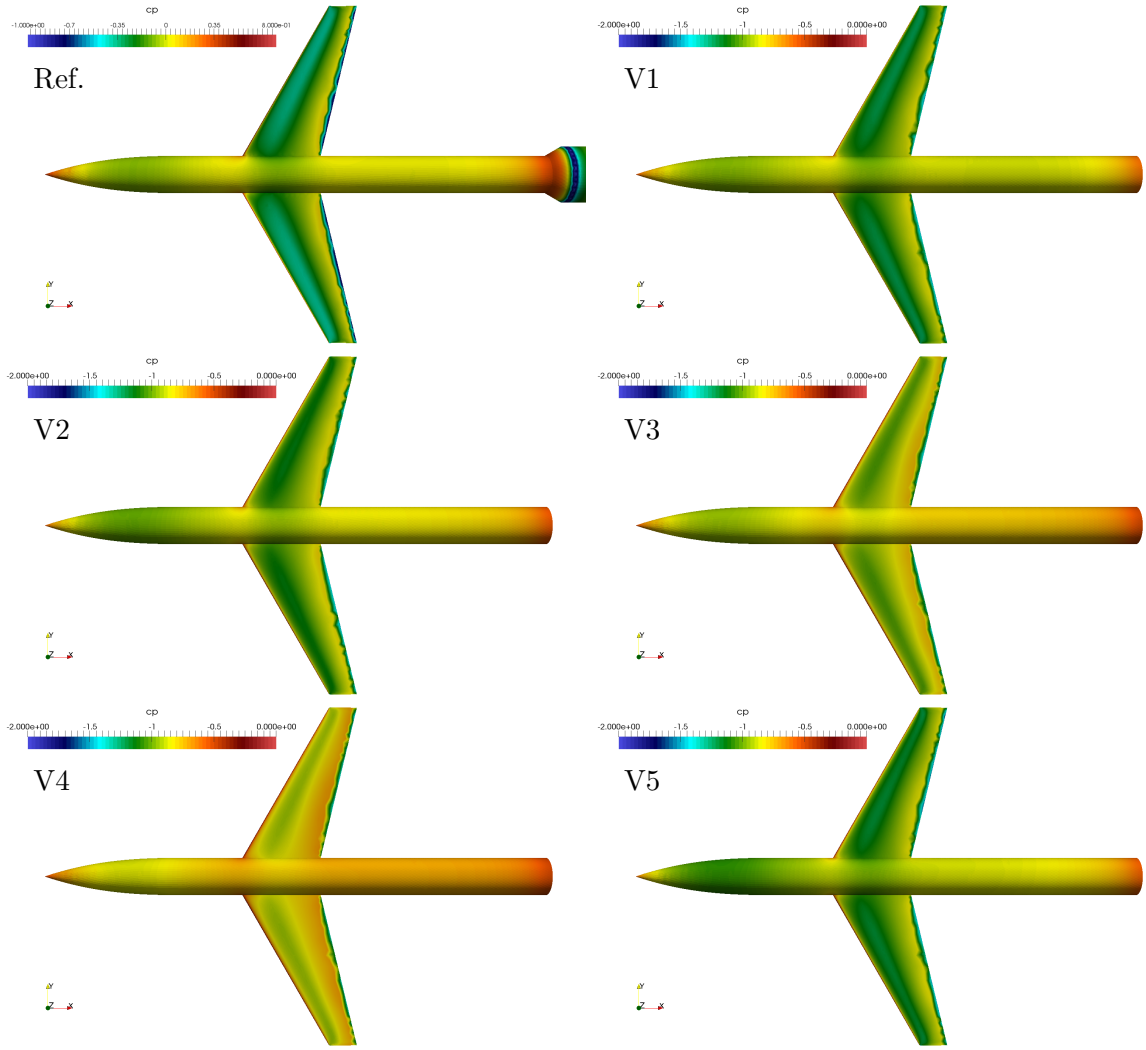

Figure 11: Sensitivity study: C_p distribution on the upper LB fuselage and wing surface for the five conducted sensitivity test flow cases.

4.2 KRG Wall-Contour Adaptation Procedure Results

Now, the wall-contour adaptation procedure and the main simulation results outcome of the performed final simulation study are discussed and presented now. Starting point is the generic LB aircraft configuration in neutral position ($\alpha = 0°$ AoA). The lower and upper test section walls had been asymmetrically pre-deformed, see the Figure 13, thereafter the first grid was generated and the whole KRG wall-contour adaptation process was initiated.
After starting with the initially set wall deformations the same TAU simulation process was conducted as in the sensitivity study described before. Again during each TAU simulation process y^+ grid adaptation step and associated pressures adjustments were performed twice. The resulting pressure conditions for getting the M = 0.8 onflow are listed in Table 4.
After finishing the TAU simulation process C_p values along the middle axis of the test-section upper and lower walls were extracted and used as input for the computation of the next KRG test section upper and lower wall contours by use of the 3D-adaptation procedure, implemented in the KRG data analysis tool "dark". Those adapted walls should deliver better flow results in regard to the goal to generate nearly free flight conditions for the model in the wind tunnel. By going back to a CAD tool the old wall contours were replaced by the new calculated contours,

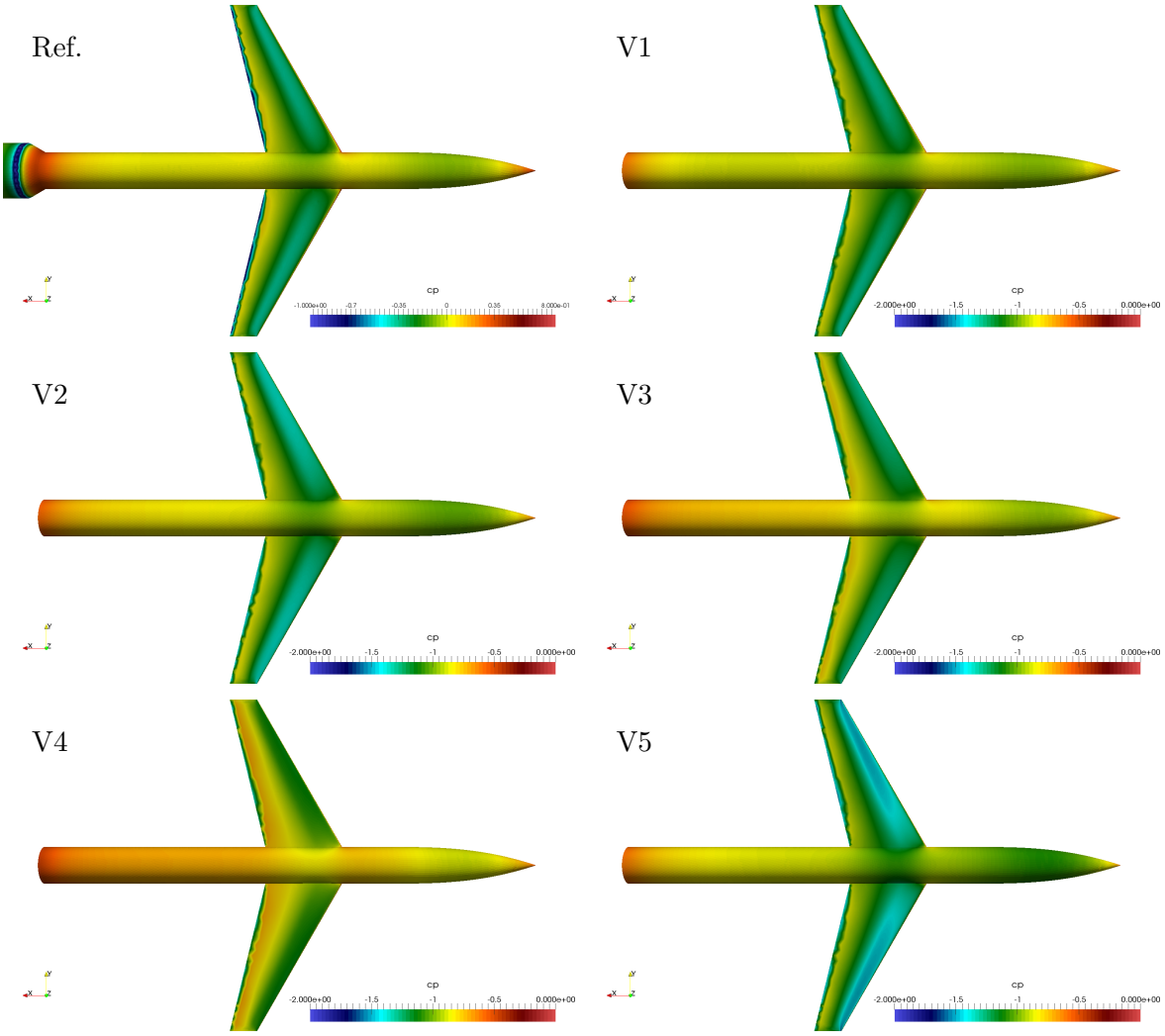

Figure 12: Sensitivity study: C_p distribution on the lower LB fuselage and wing surface for the five conducted sensitivity-test flow cases.

Table 4: Pressure Conditions of the First Wall-Contour Adaptation Study

Pressure Condition Inflow and Outflows

flow case	inflow - total pressure [Pa]	outflow - static pressure [Pa]
init. wall adap.	275000	218500
1. wall adap.	275000	200500
2. wall adap.	275000	205700
3. wall adap.	275000	208500

then the grid generation with CentaurSoft was applied again and, thereafter, a new TAU CFD simulation was started again. Afterwards, the C_p distribution were extracted from the new flow simulation results.
In most cases, after two of these entire wall-contour adaptation process loops, the described procedure is able to deliver the so targeted "interference-free wall contour". This was the case for the LB aircraft configuration in neutral position. A third wall-contour adaptation iteration

was only performed to cross-check the achieved results showing no significant improvement any more. The associated wall contours of each wall-contour adaptation step and, therewith, the wall displacement development are depicted in Figure 13 for the 0° onflow case, and in Figure 14 for the 3° onflow case.

After the simulation cycles were finished for the different wall contours, the results were quantitatively analysed. Thereto, surface C_p distributions along the fuselage symmetry axis and three spanwise cross-sectional wing cut-positions were determined and plotted. The wing-cut positions were $y_1 = 96\,mm$, $y_2 = 121\,mm$ and $y_3 = 146\,mm$. As reference for the evaluation the C_p distribution results were taken from the flow simulation results for the flow around the LB aircraft configuration under freeflight conditions with the same Mach and Reynolds number. Here, freeflight means that a CFD simulation of the flow only around the LB aircraft model was conducted without the KRG wind tunnel or any other flow restrictions.

In the top graph of Figure 15 the C_p distributions along the symmetry axis of the LB fuselage are plotted. The C_p values for the initial upper and lower wall position (red line) are qualitatively similar to the reference C_p values but quantitatively far away. After the first wall-contour adaptation a slight overshooting can be observed. The second adaptation steps shows very good results, only minor deviations are visible at the front part of the fuselage. A third wall-contour adaptation step is not really improving the results. The final deviation remains visible, here another more locally acting adaptation could perhaps improve results further more. In the lower graph of 15 the C_p distributions along the first span-wise cross sectional wing cut are plotted. The wall-contour adaptation steps are showing the same trends as for the fuselage. However, at the leading edge region of the wing the C_p values are deviating the most and the slope is less pronounced. This is a hint that there is a slight flow blockage effect left induced from the rear part of the test section, when taking the results of the sensitivity study into account. This means that the Mach number at the control points are accurately hit but in comparison to freeflight a slightly stronger Mach number slope along the wind tunnel could be observed. In regard to this relatively long configuration in comparison to the length of the test section, this can be interpreted as a hint to extend the test section, since the slope at the end of the test section can not be adjusted enough to keep the Mach number constant in flow direction over the whole length of the test section.

In Figure 16 a further comparison of the C_p distribution along two wing cuts of the LB configuration for the M = 0.8, AoA 0° onflow case are performed. An interesting trend can be observed: going from the mid sectional plane outwards in spanwise direction the results are getting worse. This means that the wall-contour adaptation procedure perfectly fits at the mid-sectional plane of the test section, because the C_p wall information taken at the centre line of the walls were fed into the wall-contour adaptation computation. The outcoming new contour is nearly perfectly shaped for the centrally placed LB fuselage, but not for further outwards lying the wing parts. The different variatiosn of the wall contour revealed that the narrower the first wall contour is the more beneficial ist it for the slim wings but less beneficial for the thicker fuselage, in contrast widener wall contour of the test section is positive for the thicker fuselage. This can be confirmed when observing the C_p distribution on the lower and upper surface of the LB aircraft configuration, see Figure 17. The C_p value results of the first wall adaptation are quite similar to the reference flow case on the wings but not for the fuselage. By conducting the second or third wall adaptation step it was tried to improve the results, however, the partially contradictory response on the adaptaion could not significantly improve the results for the wing and fiuselage parts. This differences are a direct consequence of the 2D wall-contour change, unfortunately the freedom to adapt the wall contour more locally, which would require a fully 3D wall-contour adaptation, is not given.

Nevertheless, the achieved results show that the whole conducted wall adaptation procedure, which follows its role model from the wind tunnel process, is well working. In particular, at the

Table 5: Pressure Conditions of the Second Wall-Contour Adaptation Study

Pressure Condition Inflow and Outflows

flow case	inflow - total pressure [Pa]	outflow - static pressure [Pa]
init. wall adap.	225000.0	174300
1. wall adap.	225000.0	171000
2. wall adap.	225000.0	174800
3. wall adap.	225000.0	165700
4. wall adap.	225000.0	171000
5. wall adap.	225000.0	175000

middle section, where the adaptation is made for, the procedure delivers after two wall-contour adaptation iterations reliable and very accurate results.
Now the more challenging flow case with an AoA of $\alpha = 3°$ is considered. Hereto the generic LB aircraft configuration was rotated around the spanwise axis by 3°. This also led to a very small shift of the LB model within the wind tunnel test section, which also should be compensated by the adaptation procedure. Grid generation parameters, control points for Mach number adjustments and also the whole simulation process loop were left the same. Straight walls were chosen as initial contour of the wind tunnel test section, see Figure 14. Then, as described above, again several process loops were performed. In contrast to the former a new pressure level was set in order to guarantee a new scenario and, thus, it was consciously not performed a restart. The final inflow total and outflow static pressure values, results of the Mach number adjustment, can be found in Table 5.

Again, C_p distributions along the fuselage middle plane and three wing cuts, the same as above, were compared, see Figure 18 a)-b)and 19 a)-b). It turns out that the initial, straight wall contour shows on the upper part of fuselage along the middle plane axis a quantitative good agreement to the freeflight reference flow results. However, the lower side of the fuselage does deviate. Thereafter, only a slight wall contour change was calculated, hence, the first wall adaptation flow results only slightly perform better. Again on the lower side the C_p distribution of the reference case was not hit. Thus, a second wall adaptation was initiated with a higher deformation of the lower wall. This shifted the overall C_p distribution too much. Thus a consciously exaggerated correction was put into the wall-contour adaptation system for the third wall adaptation procedure, in order to provoke a strong response. The resulting C_p values again deviated too much, now indicating too strong flow acceleration. In particular, the wide opening of the upper wall contour, see Figure 14, allows the flow to shift the shock position on the wind far further downstream in comparison to the former results. This was obviously a too strong input.
With the new information a fourth wall-contour adaptation was started which outcoming C_p results perfectly met the given reference values on both sides of the fuselage. A further last wall-contour adaptation step didn't improve the results any more, in contrast, it showed slightly worse values.
Unfortunately the results for the wing cuts are not so convincing: even more worse than in the previous AoA 0^{circ} study the C_p distribution of the reference flow case could not be reproduced by any of the adapted wall-contour changes. All, the pressure level and the shock position as well as the shock intensity are quite different. Only on the pressure side of the wing the results are quantitatively and qualitatively comparable, in particular for the last wall-contour adaptation flow case.

The obvious trends are, first, an underestimation of the suction peaks on the upper side of the wing, and, secondly, a overestimation of the pressure on the lower side of the wing. Only the consciously strong deformed third wall-contour adaptation case shows a general shift to lower C_p values but also to an elongated high Mach number flow and a delayed shock, compare the illustrated C_p contour in the Figures 20 and 21 for freeflight and the wall-contour adapted flow cases.

Nevertheless, these results do not state that the wall-contour adaptation procedure is not working. It only demonstrates that the hardware restriction, the possibility to only perform a 2D wall-contour change, is not suitable for this complex generic LB aircraft configuration, in particular when angles of attack come into play. When comparing the flow results of the best contours of the wall-contour adaptation procedure with them of the reference flow case, depicted in Figure 22, then it is clearly demonstrated that the used wall-contour adaptation algorithms and procedures are performing very well for the objective they are made for: the wall-contour adaptation for the flow around a quasi 2D pure wing configuration.

The reason for the problems when applying the wall-contour adaptation on the flow around complex 3D configuration, which is represented by the generic LB configuration, is first, a lack of adaptivity to larger scale 3D flows occurring at the outer regions of the test section, and, secondly, the problem of flow blockage. Both effects can be observed in Figure 23, where besides the C_p distribution on the LB configuration the Mach number contour is depicted on a vertical cutting plane through the test section at the wing mid-chord position. It is obvious that the high Mach number flow region is artificially restricted by the test section side wall, also here the best wall-contour adaptation case is used for comparison. The evaluation of these results leads to the conclusion, that, besides the necessity for more complex 3D wall-contour adaptation in spanwise direction, is that another possibility is to further downscale the used wind tunnel model avoiding the occurrence of flow blockage.

5 Conclusions

The objective of this CFD simulation study was to cross-check the wind-tunnel wall-contour adaptation procedure, used in DNW–KRG wind tunnel experiments. Therefore, the same procedure as used in experiments was rebuild in the virtual environment of the iterative simulation process chain from CAD preparation, grid generation over flow simulation, data analysis and wall-contour adaptation. The focal point was to investigate CFD simulation strategies in order to get valid results with respect to the wall-contour adaptation procedure conducted in KRG wind tunnel experiments in the future. Eventually it could be demonstrated that the described iterative process was able to adjust the wind tunnel test section upper an lower wall contour so that along the middle axis a quite "interference-free" flow occurred.

Nonetheless, the simulation process was not as easy as though in the beginning of the study: it has to be remarked that the results of the wind tunnel simulation campaign are very sensitive to the order of the solving algorithm and the used discretisation operator. The shock position depends strongly on that. Two cycles of y^+ adaptation had been performed, in each cycle the correct Mach number model onflow conditions at distinct measurement positions had to be manually adjusted by corresponding exit pressure values during the simulation study. No automatic optimization was used, therefore there is further optimization potential for accelerating future studies. Even more, in particular the spatial resolution at the shock position was of crucial importance as the CFD grid study revealed. Only with the fine grids used in this study the present results could be achieved. This increased the computational effort drastically, Nevertheless, a higher spatial resolution would even be better in regard to the quantitative results, the restriction of computational memory and effort prevented further refinement. However, the qualitative results would barely change.

In fact the C_p distributions along the middle axis of the fuselage of the flow under freeflight conditions could be very well reproduced by applying the wall-contour adaptation procedure, implemented in the DNW-KRG data analysis software "dark". However, the results revealed also that the 2D restriction of the real wall-contour adaptation mechanics, as it is implemented in the DNW–KRG wind tunnel and transferred in this simulation study, is not able to reproduce the freeflight flow results at the wing parts in case of an even small angle of attack of 3° for the considered generic LB aircraft configuration. In fact, only when symmetry conditions, in regard to the onflow, are given the C_p distribution on the wings is nearly the same as for the freeflight flow results.
For this type of aircraft configuration with this typical geometric fuselage-wing ratio it can be stated that it is very sensitive to asymmetric onflow conditions due to the flow displacement by the fuselage, thus, it is barely impossible to achieve freeflight conditions on the wings. In general this is valid at locations, which are further away from the middle axis of the wind tunnel test section. The qualitative comparison of the Cp distributions for the sequence of wall-contour dependent flow results and the Mach number distribution on a cross-sectional cut at the wing mid-chord position indicates that the flow blockade effect is enforced under AoA flow conditions. Latter cause an observable flow displacement and acceleration in particular closer to the wind tunnel lower and upper but also to the side walls of the KRG test section. This blockage effect can only be reduced by two measures: the first would be to reduce the model size, which in general is not always possible, the second would mean to go from purely 2D wall-contour adaptation to a new more flexible kind of 3D wall-contour adaptation. This step is comparatively easy in the virtual environment of the simulation process applied in this study but not under the real and hard conditions and constrains of a real wind tunnel as the cryogenic wind tunnel. This study has opened additional aspect for future work: A simulation study for investigation and development advanced 3D wall-contour adaptation concepts should be initiated as the next logical step for the improvement of the DNW-KRG wind tunnel.

References

[1] J.R. Edwards and S. Chandra. Comparison of Eddy Viscosity-Transport Turbulence Models for Three-Dimensional, Shock-Separated Flowfields. 34(4), 1996.

[2] T. Gerhold, O. Friedrich, J. Evans, and M. Galle. Calculation of Complex Three-Dimensional Configurations Employing the DLR-TAU-Code. AIAA-97-0167, AIAA 35^{th} Aerospace Sciences Meeting & Exhibit, (Reno, NV), 6–10 January 1997.

[3] H. Holst and K. S. Raman. 2-d Adaptation for 3-d Testing. Interner Bericht 29112-88 A 03, DFVLR, 1988.

[4] S. Koch. Zeitliche und räumliche Turbulenzentwicklung in einem Rohrwindkanal und deren Einfluss auf die Transition an Profilmodellen. Forschungsbericht DLR FB 04-19, DLR, 2004.

[5] H. Ludwieg. Der Rohrwindkanal. *Z. Flugwiss.*, 3(7):206–216, 1955.

[6] H. Rosemann. The Cryogenic Ludwieg-Tube at Göttingen. In *Special Course on Advances in Cryogenic Wind Tunnel Technology*, AGARD-R-812, (Cologne, Germany), 20–24 May 1996.

[7] H. Rosemann, E. Stanewsky, and G. Hefer. The cryogenic ludwieg-tube of DLR and its new adaptive wall test section. AIAA-95-2198, AIAA 26^{th} Fluid Dynamics Conference, (San Diego, CA), 19–22 June 1995.

[8] D. Schwamborn, A. Gardner, von Geyr, A. H., Krumbein, H. Lüdeke, and A. Stürmer.

[9] D. Schwamborn, T. Gerhold, and R. Kessler. The DLR-TAU Code - an Overview. In *Proceedings of the ONERA-DLR Aerospace Symposium ODAS*, (Paris, France), 21–24 June 1999.

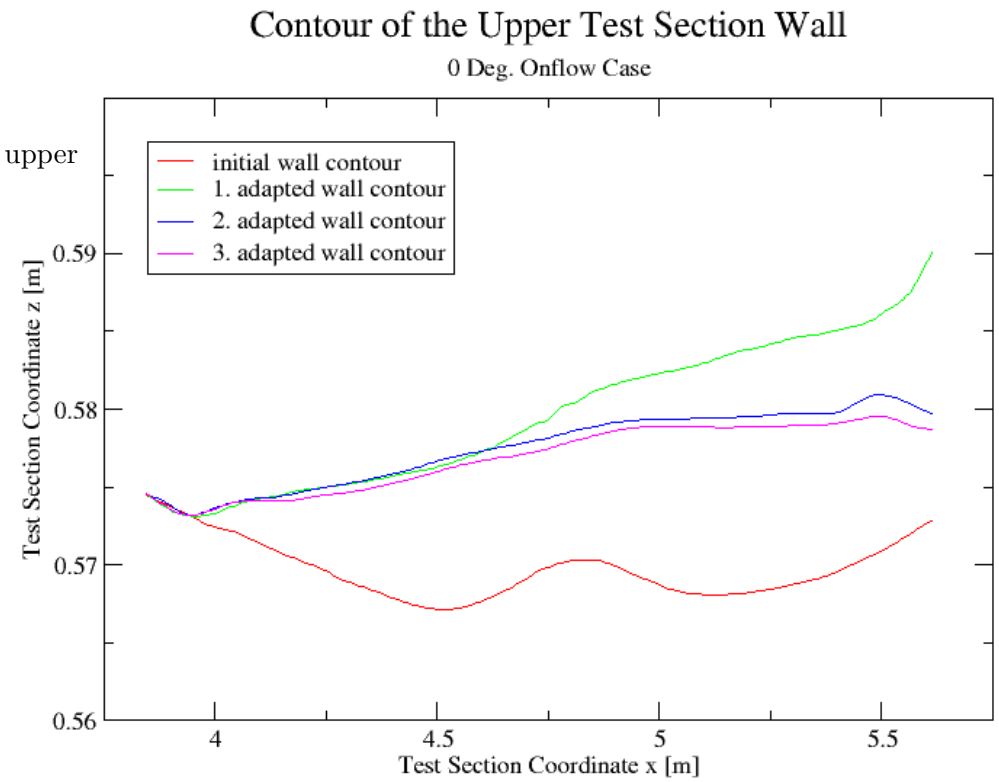

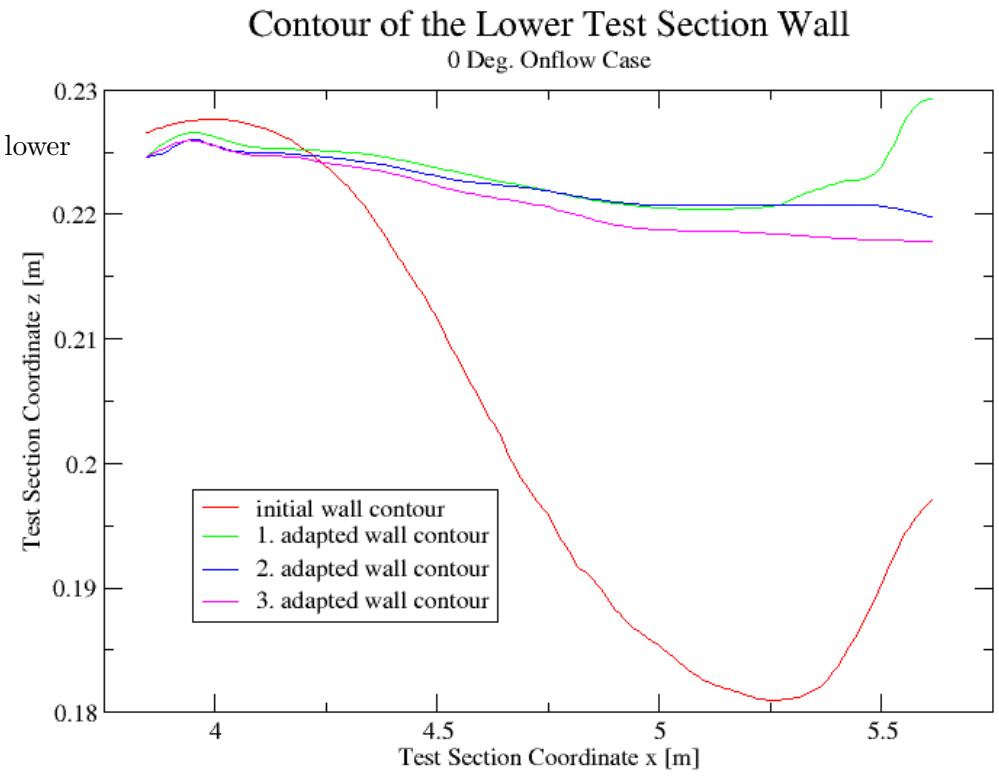

Figure 13: 0° onflow case: initial and wall-adapted test-section wall contours

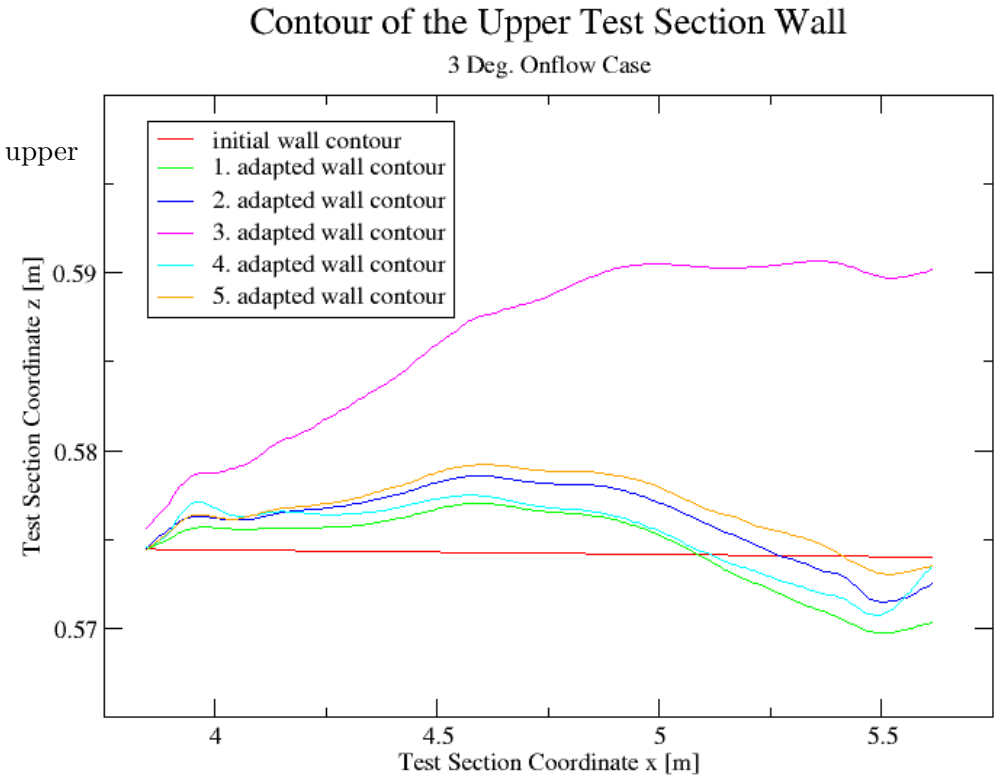

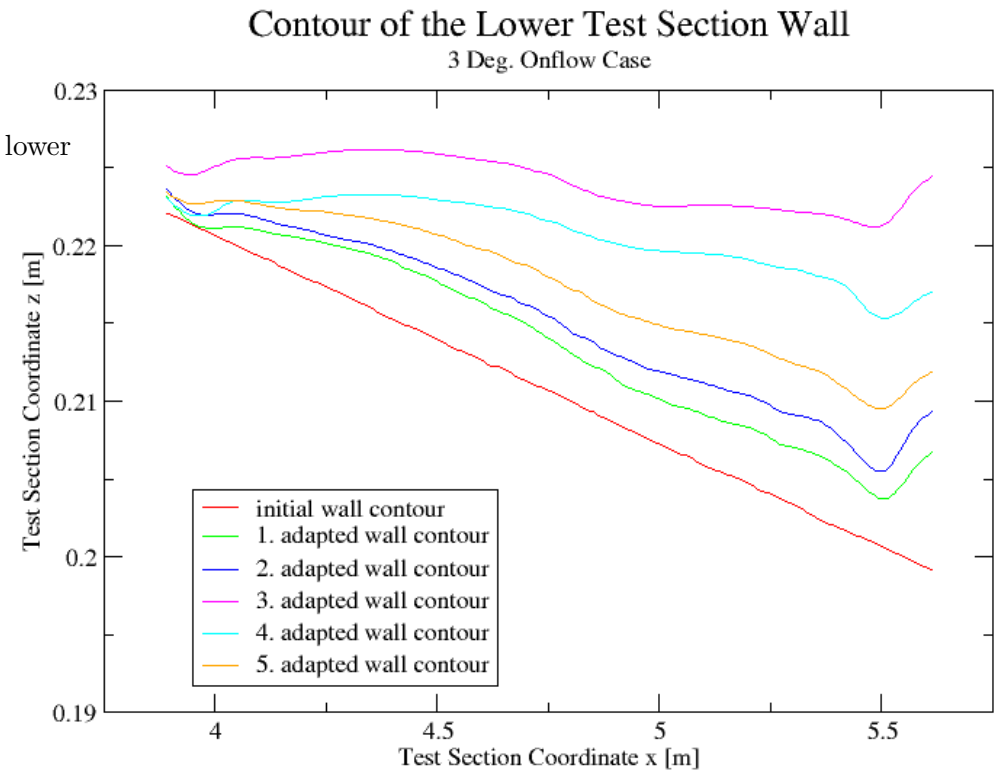

Figure 14: 3° onflow case: initial and wall-adapted test-section wall contours

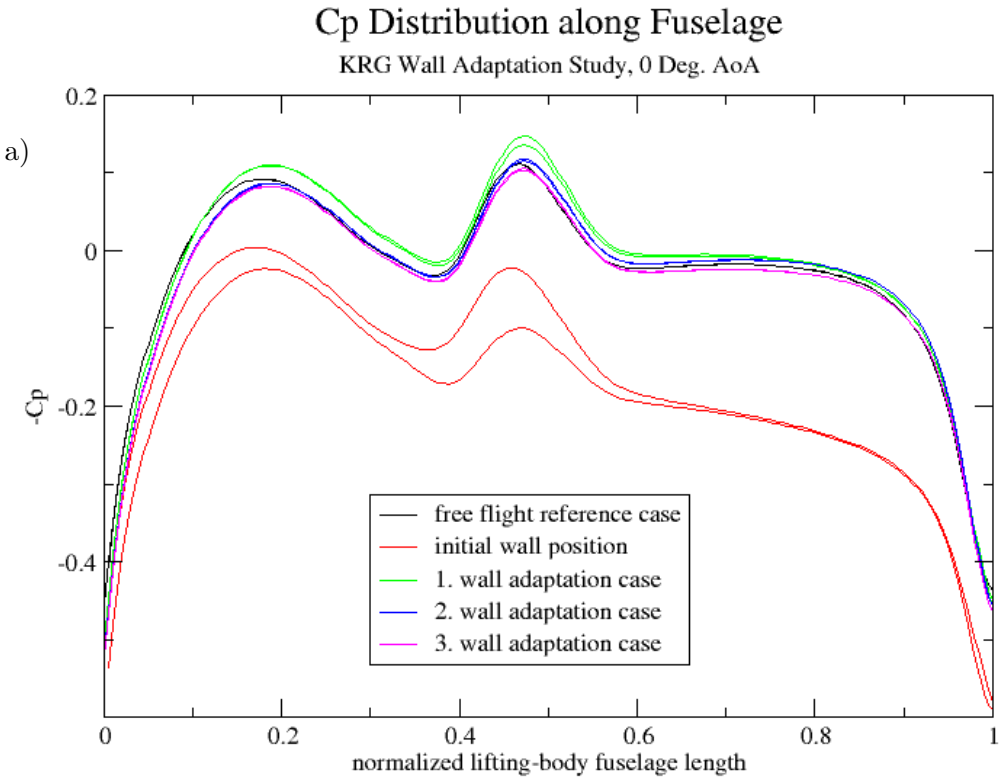

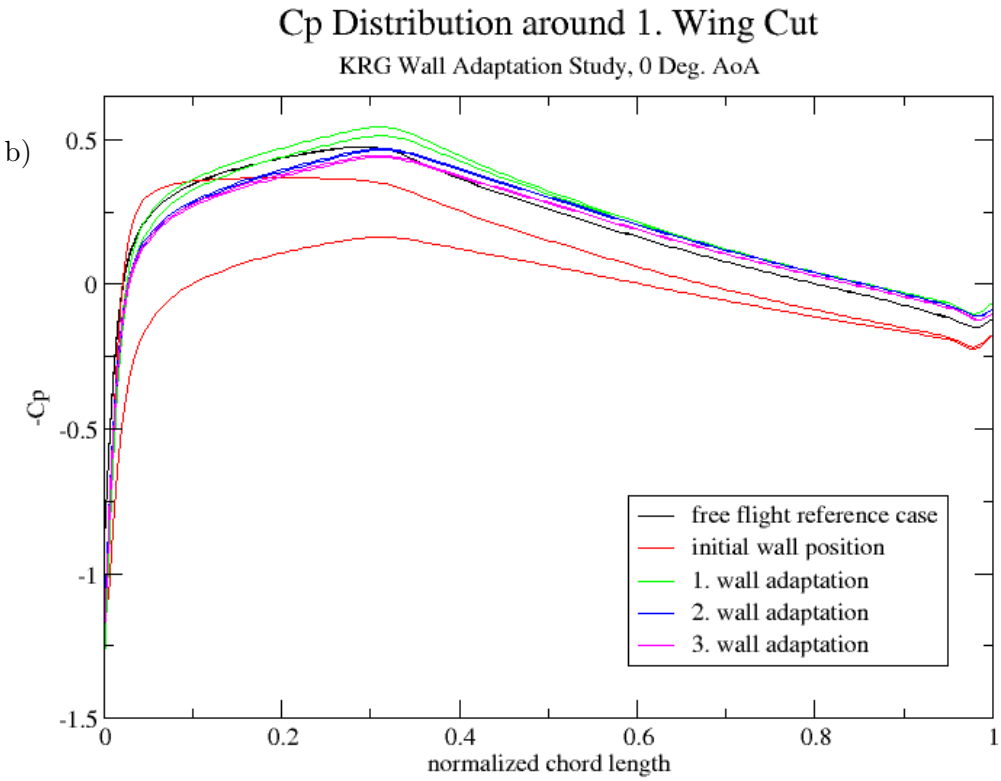

Figure 15: M = 0.8, AoA 0°, wall-contour adaptation depending C_p distribution along LB cut-planes: mid, 1. wing cut

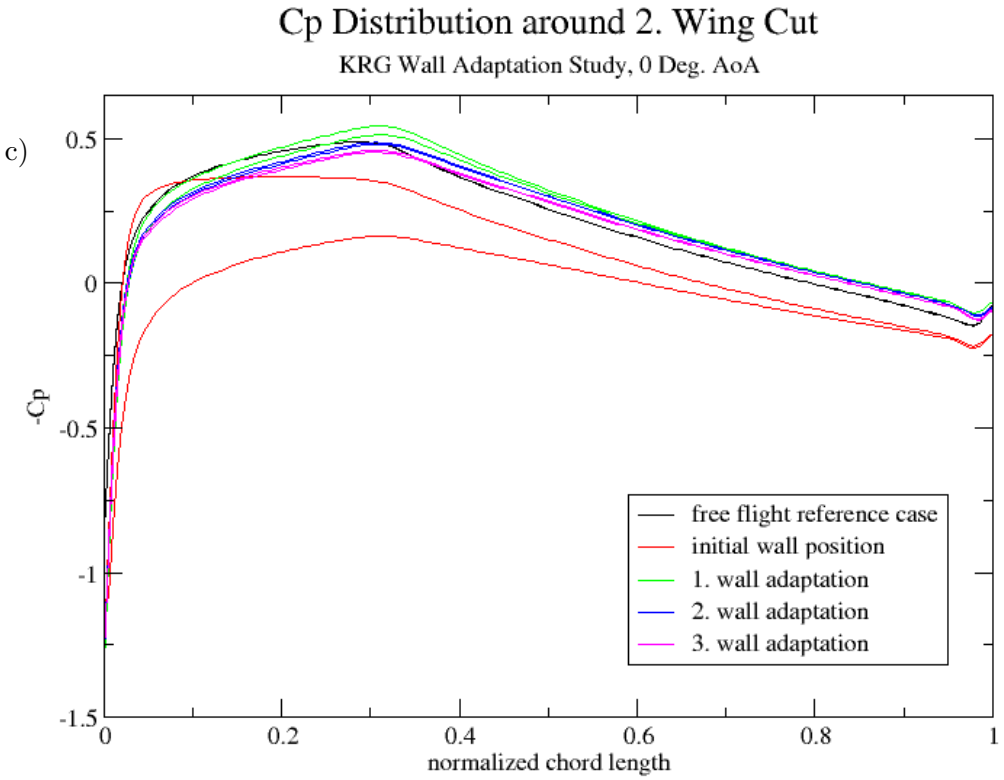

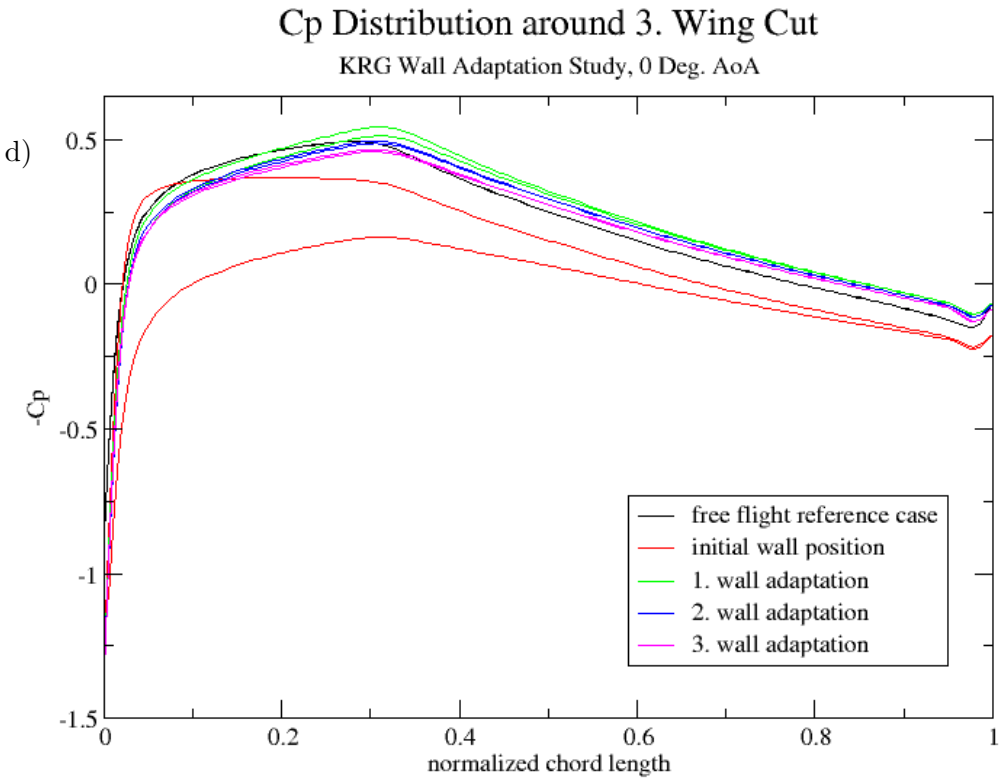

Figure 16: M = 0.8, AoA 0°, wall-contour adaptation depending C_p distribution along LB cut-planes: 2. and 3. wing cut

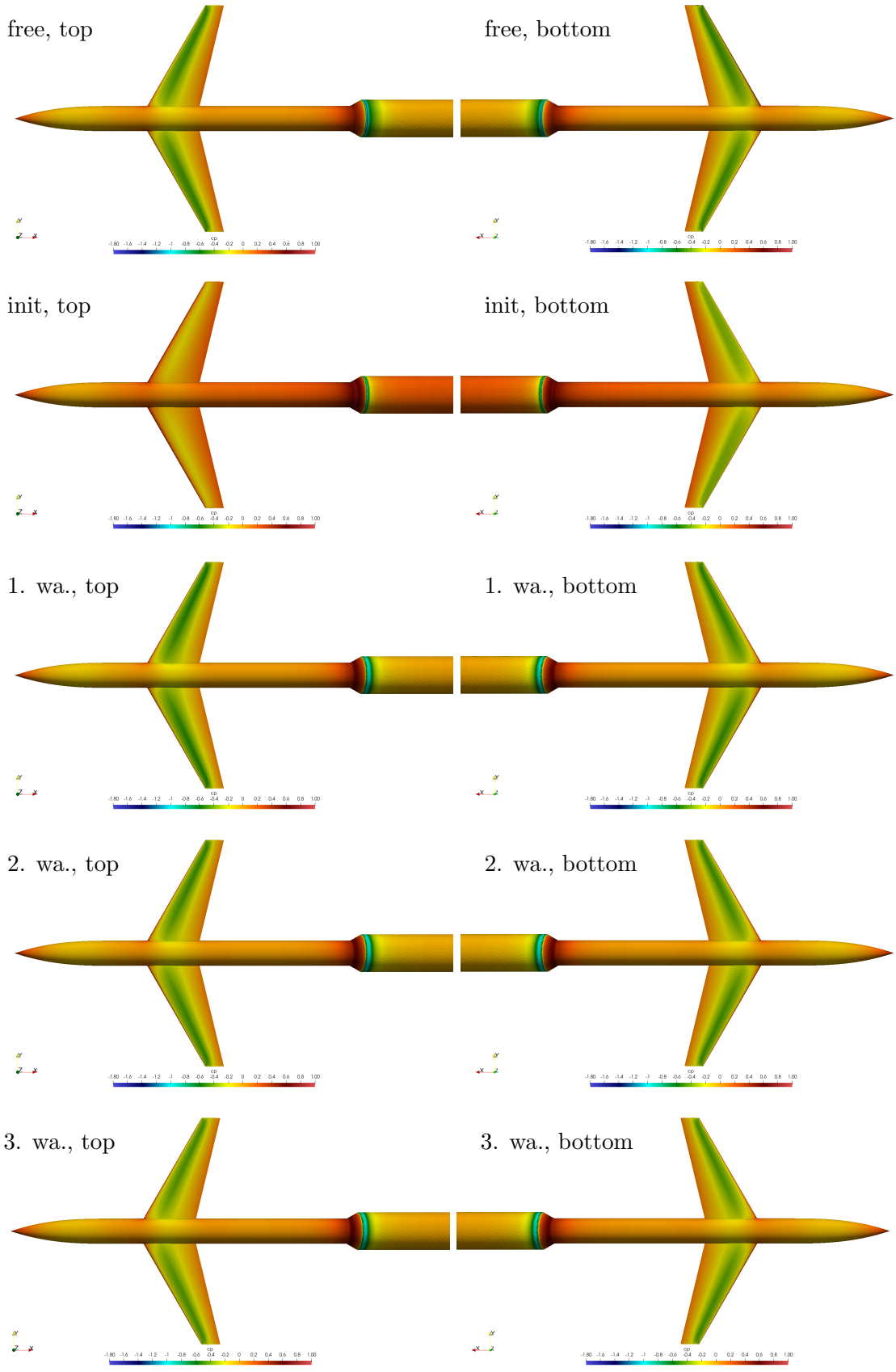

Figure 17: M = 0.8, AoA 0°, C_p distribution over the LB surface

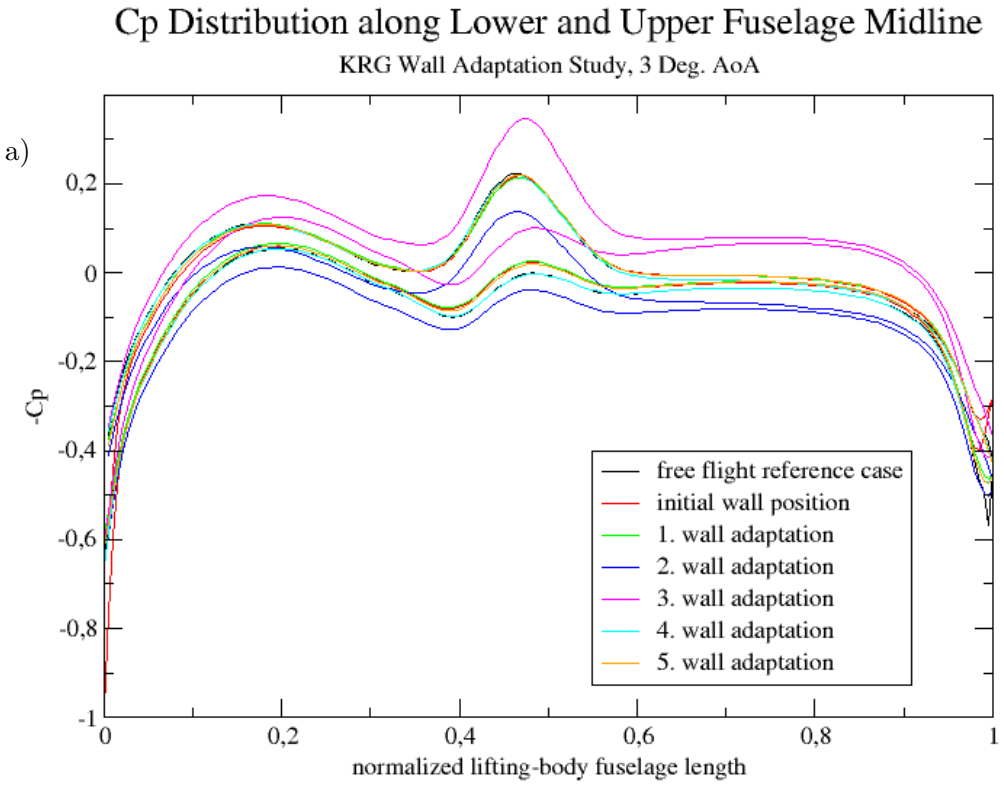

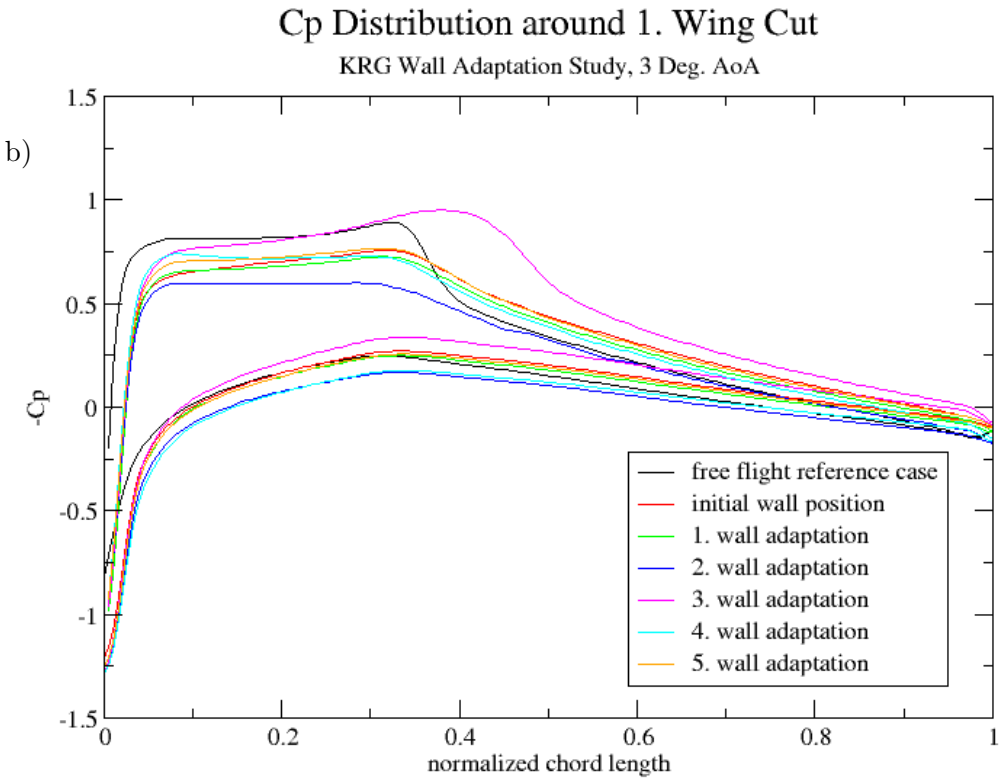

Figure 18: M = 0.8, AoA 3°, wall-contour adaptation depending C_p distribution along LB cut-planes: mid, 1. wing cut

a)

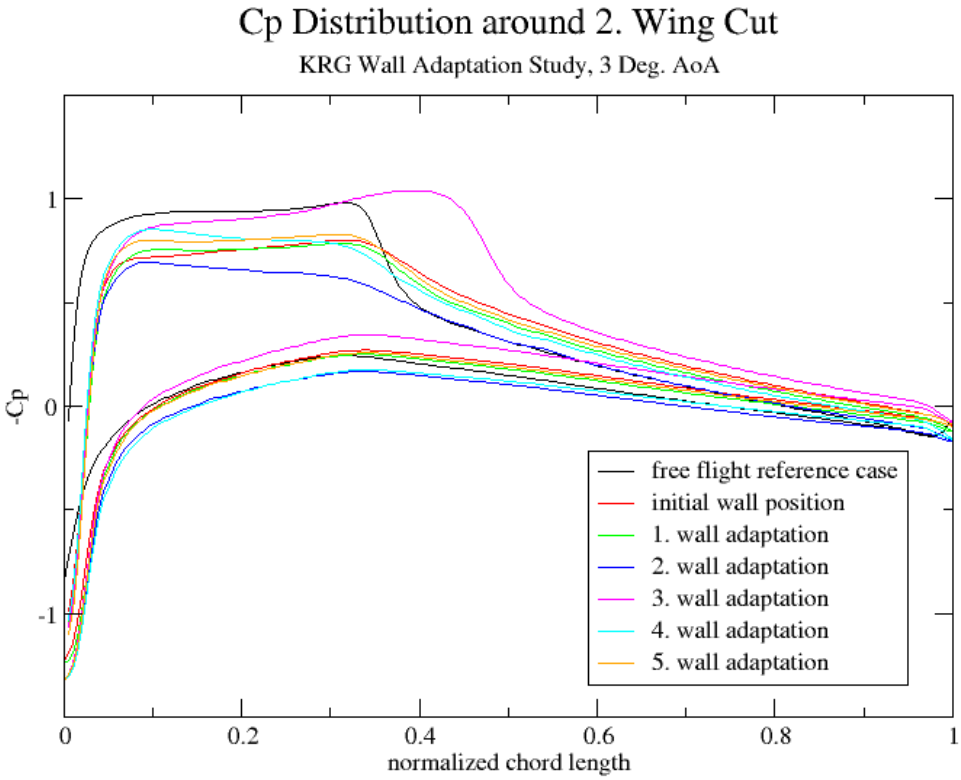

b)

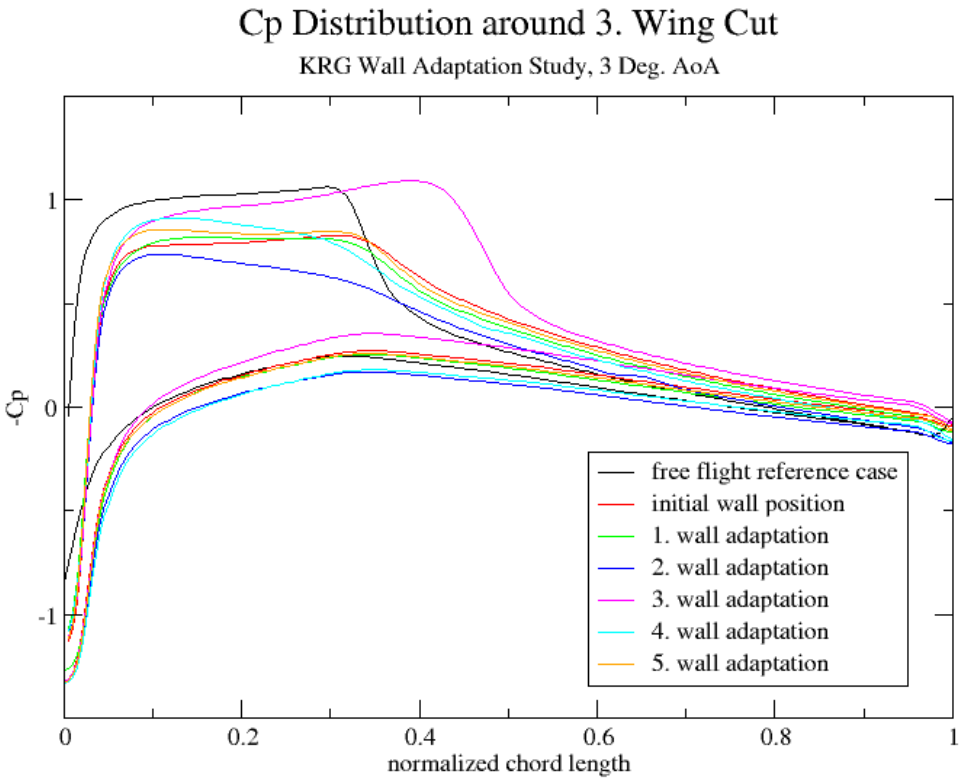

Figure 19: M = 0.8, AoA 3°, wall-contour adaptation depending C_p distribution along LB cut-planes: 2. and 3. wing cut

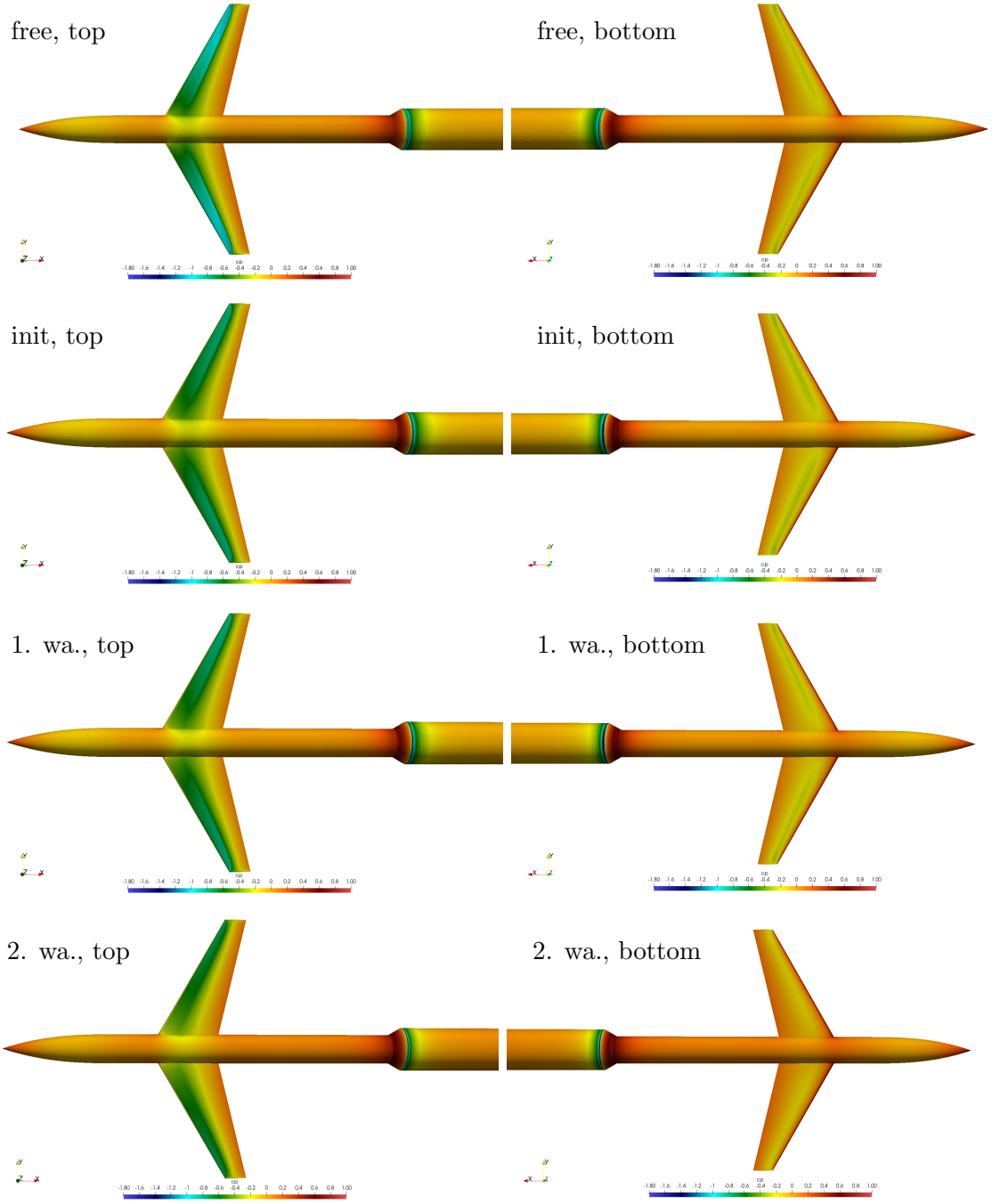

Figure 20: M = 0.8, AoA 3°, wall-contour adaptation depending C_p distribution over the LB surface (I)

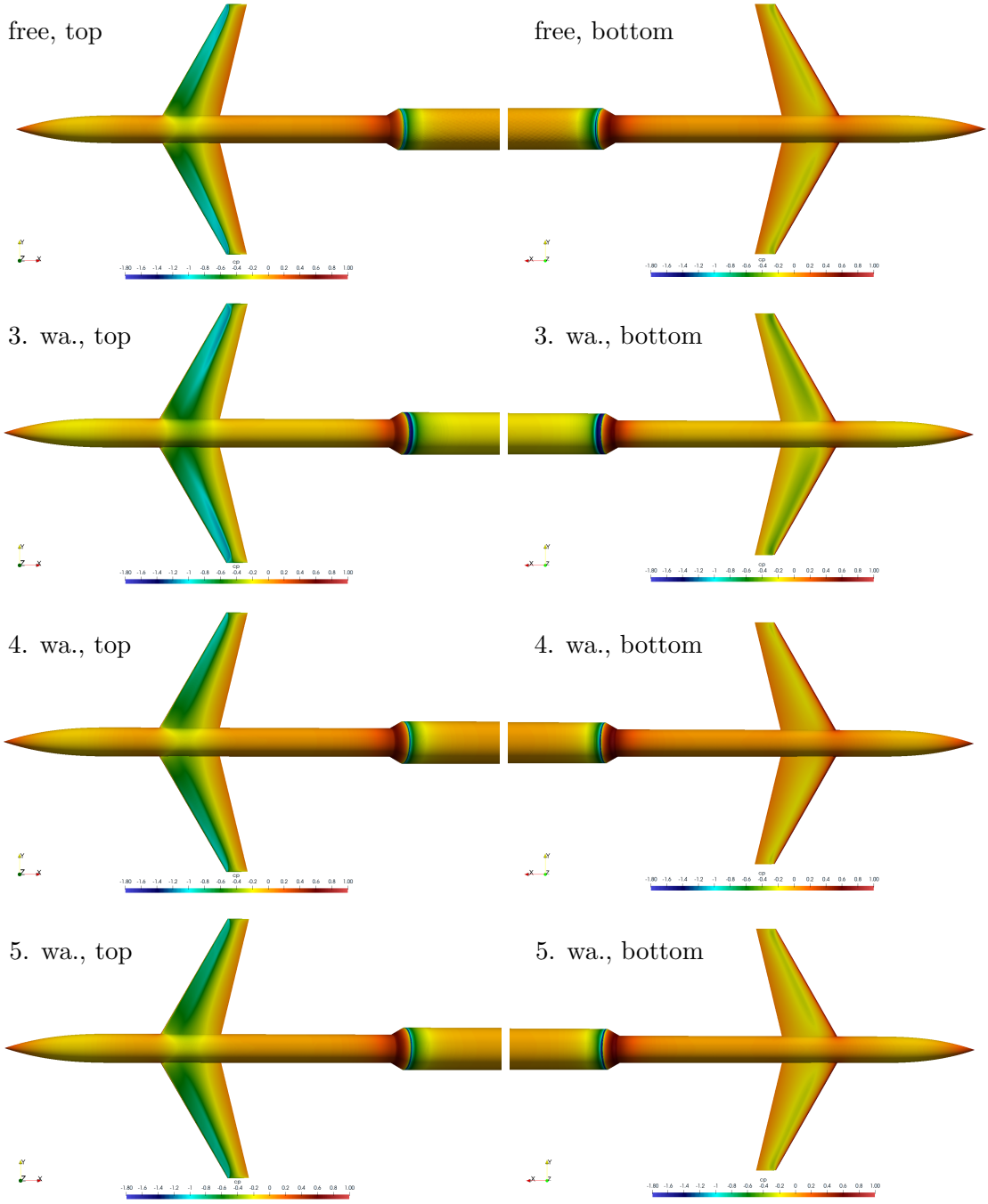

Figure 21: M = 0.8, AoA 3°, wall-contour adaptation depending C_p-value distribution over the LB surface (II)

a)

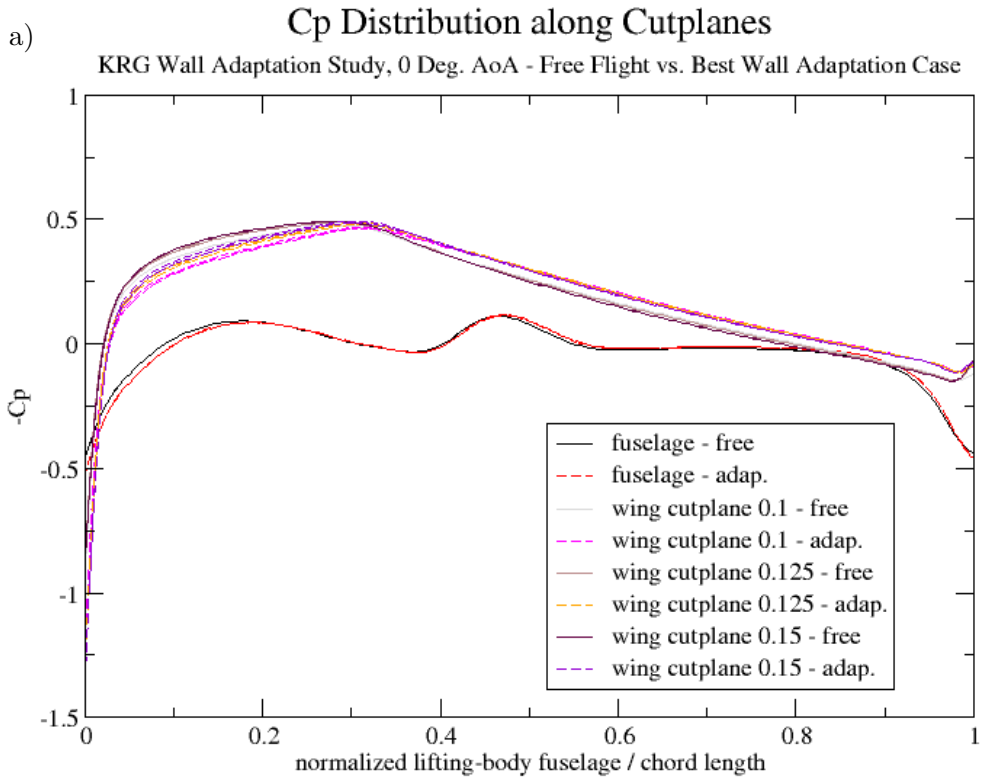

b)

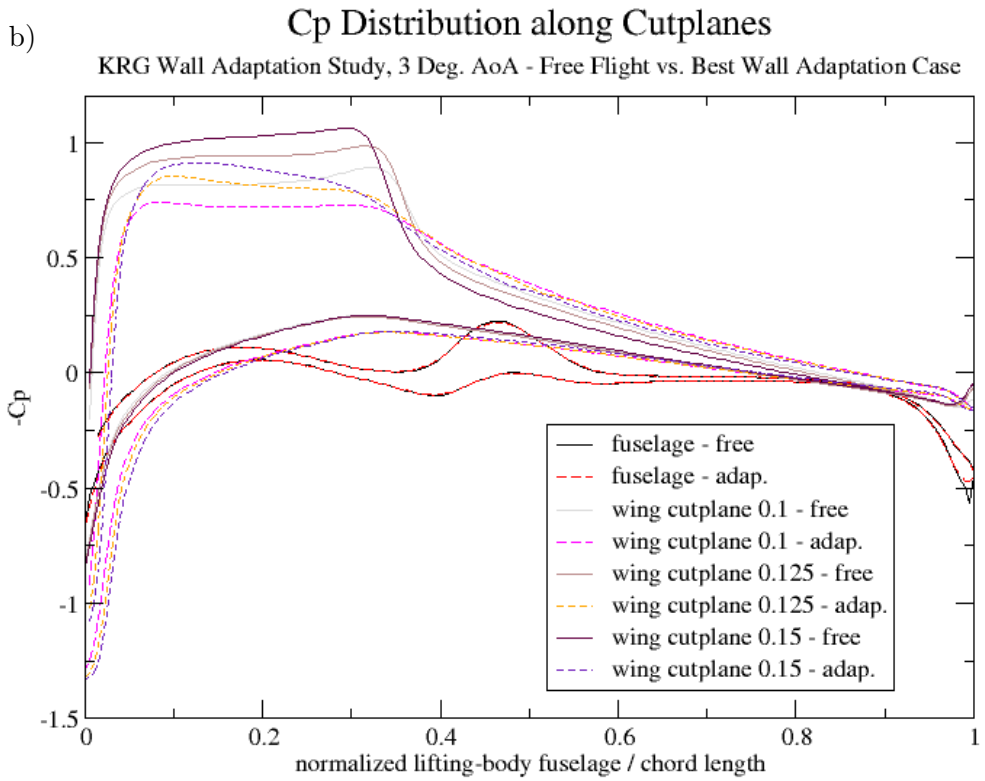

Figure 22: M = 0.8, AoA 0°, wall-contour adaptation depending C_p-value distribution along LB cut-planes

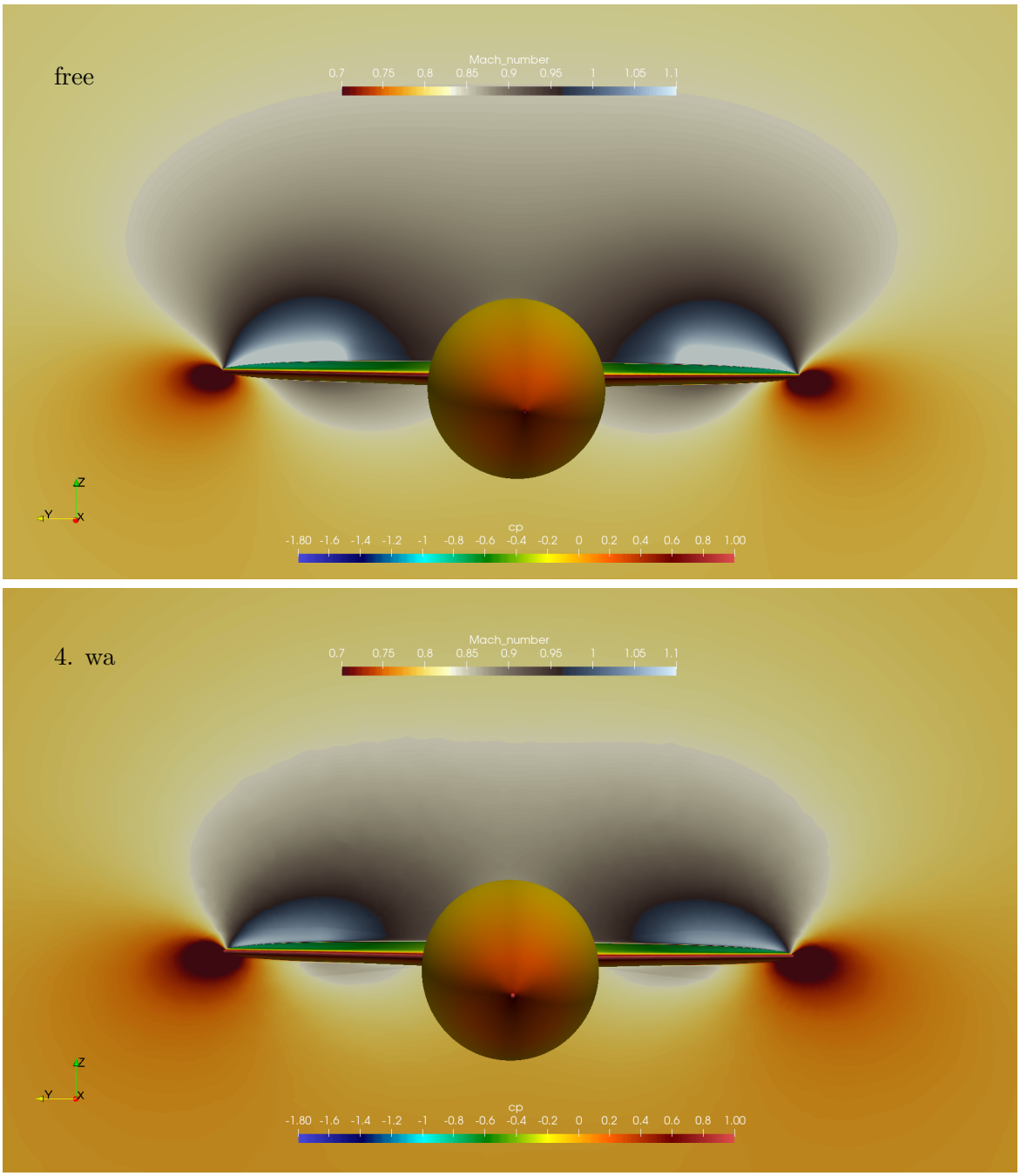

Figure 23: M = 0.8, AoA 3°, comparison of the Mach number distribution on a stream-normal cross-sectional cutting plane at wing mid-chord position, top: freeflight reference, bottom: 4. wall adaptation case (best)